Waves on Opposing Currents: Data Report

by

ARUN CHAWLA
AND
JAMES T. KIRBY

RESEARCH REPORT NO. CACR-99-03
MAY, 1999

WORK SUPPORTED BY SEA GRANT, DELAWARE

CENTER FOR APPLIED COASTAL RESEARCH
UNIVERSITY OF DELAWARE
NEWARK DE 19716

Contents

List of Tables

List of Figures

1 Introduction

Wave blocking is a phenomenon in which the energy of propagating waves is stopped by a strong opposing current. As waves propagate into opposing currents, their group velocity reduces leading to the waves shoaling on the current. If the current is strong enough then this group velocity could go to zero causing the waves to get blocked. This is fairly common at the entrances of river inlets where tidal currents can become very strong. One such example of wave blocking is shown in Figure 1. The photograph has been taken three hours after high tide, and thus, there is a strong current propagating out of the inlet. This strong current blocks waves that are trying to propagate into the inlet. Due to the sharp increase in wave steepness prior to blocking, the wave environment tends to become very rough, as can be seen in Figure 2. This causes considerable navigational hazards and boats have been known to capsize trying to cross the inlets under such circumstances.

There are many references in the literature on the dynamics of strong wave-current interactions. Bretherton and Garrett (1969) have shown that in the presence of a current it is the wave action that is conserved and not the wave energy. However, this conservation principle is based on ray theory approximations and fails close to the blocking point which is a caustic. Smith (1975) obtained a uniform solution for the wave amplitude through the blocking region. He showed that around the blocking region the amplitude envelope is given by an Airy function, and away from the blocking region the wave field consists of an incident wave and a much shorter reflected wave. Peregrine (1976) obtained the same results with the help of stream functions. Lately Shyu and Phillips (1990) and Trulsen and Mei (1993) have extended the results to include the effects of surface tension which, if the reflected waves are short enough, leads to the waves being reflected again from a second reflection point.

All these theories are based on the linear wave assumption and require that the incident waves be very small. In inlets these conditions are rarely satisfied and most waves break at or before the blocking point without getting reflected. Even those waves which do not get blocked lose a considerable amount of energy due to waves breaking on the strong currents. As opposed to depth limited wave breaking, there is a scarcity of experimental data to study current limited wave breaking. Lai *et al.* (1989) have studied the kinematics of the strong interaction between waves and opposing currents but do not give any results about the dynamics.

Figure 1: Wave Blocking at Indian River Inlet, DE USA

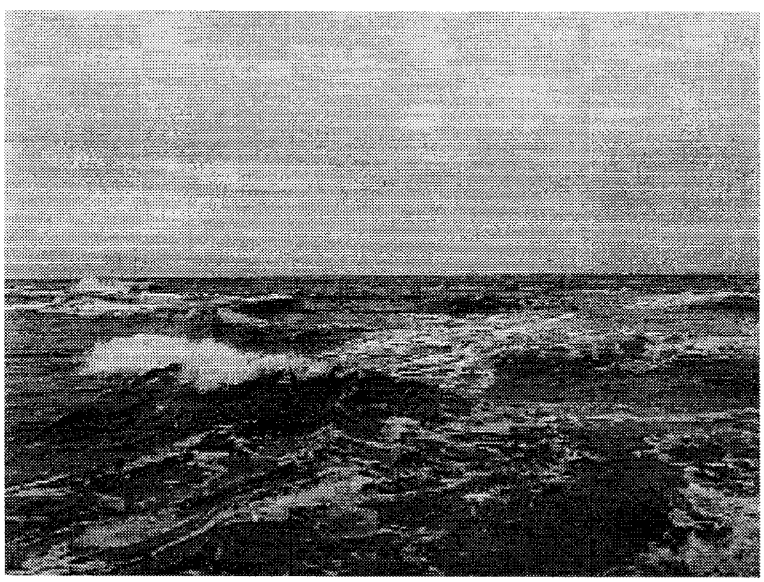

Figure 2: Wave field close to the blocking point

To develop a better understanding of the dynamics involved in the interactions between waves and strong opposing currents, a series of experiments have been conducted at the Center for Applied Coastal Research. The study is broadly divided into three parts -- monochromatic wave tests, random wave tests using fairly broad TMA spectra, and narrow spectral tests which lead to modulating wave trains. The tests range from conditions where the waves are blocked and reflected to conditions where there is steepness limited wave breaking as the waves shoal on an opposing current.

The purpose of this report is to catalog all the experiments. The report consists of a main part where the experimental setup and the different experiments are described in details. The second part of the report consists of the Appendices which contain the naming convention used for the different experiments, the gage coordinate positions and the figures from all the tests. Due to the voluminous nature of the report only the main section and the two Appendices describing the naming convention and gage coordinates are available in print form. The remaining Appendices containing all the figures may be obtained by request or by anonymous ftp from **coastal.udel.edu**. The report together with its Appendices is stored in **pub/reports**.

2 Experimental facility

The experiments were conducted in the Center for Applied Coastal Research at the University of Delaware. The aim was to simulate the conditions experienced in inlets during the periods when there are fast tidal currents propagating out of the inlet. Tidal currents are turbulent and, compared to gravity waves, vary over much longer time scales. Thus, in our experiments we generate turbulent currents with a constant mean velocity. Since we wish to isolate the phenomenon of wave blocking, the experiments have been conducted in one dimension only.

2.1 Experimental setup

The experiments were conducted in a 30 m long recirculating flume, and a schematic plan view of the setup is shown in Figure 3. Currents are generated with the help of a pump which draws out water at the rate of 0.09 m^3/s from behind the wave paddle and puts it back into the flume at the other end. A flow straightener has been placed in the flume to remove all the large scale

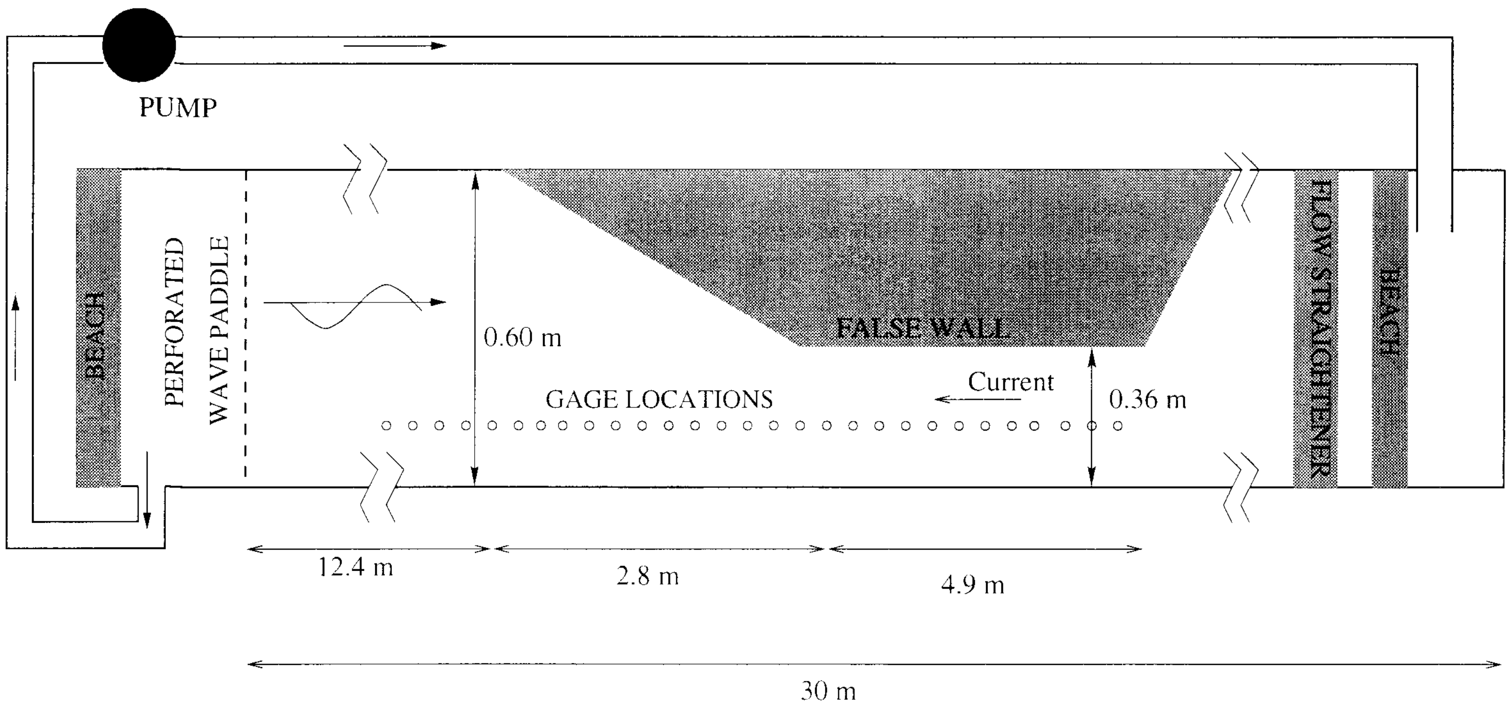

Figure 3: Schematic plan view of the experimental setup

eddies that are generated when the water enters the flume. A perforated "piston-type" wave paddle is used to generate waves in the tank. This allows us to draw out the water from behind the wavemaker, and the vertical profile of the current in front of the wave paddle remains unchanged. The width of the flume is 0.6 m and all the experiments are conducted in a water depth of 0.5 m. The wave periods range from 1.2 – 1.6 s. Thus, the experiments have been conducted in deep to intermediate water depths.

An inlet is constructed by narrowing the width over a section of the flume with the help of a false wall. The width of the narrow channel is 0.36 m. The channel expands slowly to the width of the flume to prevent flow separation in the expansion. Thus, the additional complexity of waves focusing on a laterally growing jet are avoided. The mean current varies from 0.53 m/s inside the inlet to 0.32 m/s away from the inlet. The experiments have been designed such that wave blocking occurs close to the narrow part of the inlet.

An acoustic doppler velocimeter is used to measure the current velocities, while capacitance wave gages are used to measure the time series of the water surface. The surface gage measurements extend from outside the inlet to the end of the narrow part of the inlet and are shown in Figure 3.

2.2 Coordinate system

The origin is placed at the beginning of the narrow part of the inlet with the $x-$ coordinate axis pointing down the length of the flume and positive in the direction of the waves. Thus, the inlet begins at $x = -2.8$ m, and the narrow part of the inlet extends from $x = 0$ till $x = 4.8$ m. Due to symmetry the side wall of the flume becomes the center line of the inlet. The $y-$ coordinate axis points positive towards the false wall with $y = 0$ at the centerline (right wall of the tank). The $z-$ coordinate axis points positive upwards with $z = 0$ at the still water level.

2.3 Data collection

Two different types of instruments have been used for collecting data. The particle velocities have been measured with the help of an acoustic doppler velocimeter (ADV). The velocimeter measures the horizontal velocities only. Since the currents in the experiments are fairly strong there is very little noise and the ADV works very well. The disadvantage with the ADV is that its maximum sampling rate is only 25 hz and thus is not useful for studying the turbulence structure of the current. Nevertheless, it gives very good mean velocity profiles. Data collection for the ADV is done with the help of a PC.

Apart from the ADV, capacitance wave gages have also been used in the experiments. These gages measure the time history of the water surface by giving out a voltage which changes with water level. The gages are calibrated so as to be able to convert the time series from volts to centimeters.

Both the calibration and collection of data from the gages is done with the help of a Concurrent 7200 data acquisition computer system. The computer system contains 80 A/D channels which converts the analog signals from the wave gages into digital signals. A Fortran program called **Take_data** is used to retrieve the information from the channels at a particular sampling rate and store them in individual data files. Unlike the ADV, there is no limit to the rate at which data can be sampled, and the sampling rate typically varied between 50 – 100 hz.

Gage calibration is done by moving the wave gages up and down in still water, and measuring the voltage at 1 cm intervals. To automate the process, stepper motors have been attached to each gage wire. These stepper motors are also controlled by the Concurrent 7200 computer system. Calibration is done with the help of a Fortran program called **Gcal**. To move the stepper motors, **Gcal** uses three A/D clocks. One of the clocks moves the motors through the specified distance between calibration points. The second clock collects the data at each point (100 samples at 100 hz). And the third clock changes the direction of the motors when the total number of calibration points in a particular direction (as specified by the user) have been completed. All the readings are taken with reference to the still water level and a regression analysis carried out. All the gages are sturdy and the calibration curves are linear. A typical calibration curve for 4 gages is shown in Figure 2.3. Changes in water temperatures affect the calibration curves slightly and calibration must be done at least once a day. In our experiments, calibration of the gages was done every time the gages were moved so as to ensure the proper functioning of the gages. Thus, typically calibration of the gages was done 3 to 4 times a day.

The Concurrent 7200 computer system is also used to run the wavemaker. It has 4 D/A boards, and one of the boards is connected to the wavemaker. A Fortran program **Send_data** converts a given paddle time series into an analog signal at the required sampling frequency (specified by the user), which then move the wave paddle. The sampling frequency for moving the wavemaker was around 4000 hz for our experiments, eliminating the need for

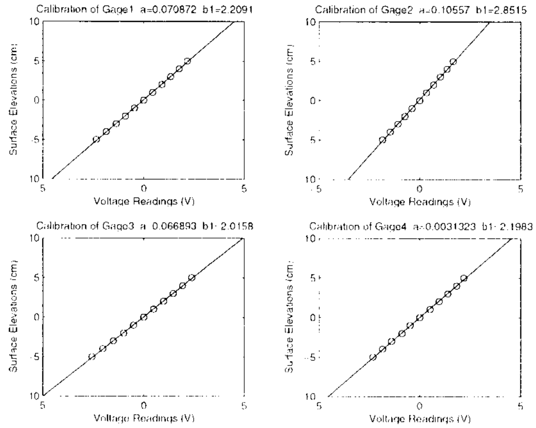

analog filtering of the command signal.

2.4 Current profiles

To determine the variation of the current in the flume, a detailed measurement of the current vertical profile was done at various locations in the channel. At each position the horizontal velocity in the x direction has been measured as a time series with the help of the ADV. Data sampling has been done at 25 hz for 330 s. The mean current profiles are shown in Figures 4 - 8, where b refers to the channel width and U refers to the mean velocity defined by

$$U \equiv < u(t) > \tag{1}$$

The measurements have been taken for two cases - when there are only currents, and when there is a strong monochromatic breaking wave propagating against the currents. The incident wave corresponds to the Test 6 case for the monochromatic breaking wave tests. There is a considerable amount of wave breaking but the wave does not get blocked by the current. The aim is to check if the mean velocity profile varies across the channel both in the presence and absence of large waves. From the figures we see that there are some variations in the y direction away from the inlet, but inside the inlet this variation is minimal, particularly close to the narrow part of the inlet where all the wave blocking takes place. We make the assumption that variations across the channel are negligible and integrate out the y dependency to simplify our study. Apart from measuring the mean current, the turbulence in the current was also determined. The turbulence has been defined as

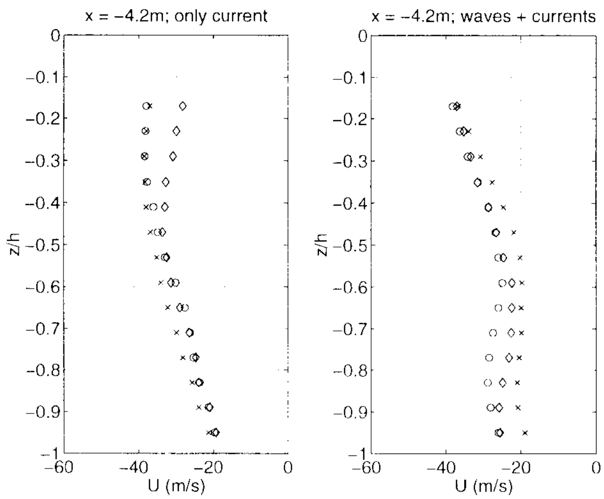

Figure 4: Mean velocity profiles at $x = -4.2$m;'○' $y/b = 0.25$,'×' $y/b = 0.5$,'◇' $y/b = 0.75$

$$\tau \equiv \sqrt{< (u(t) - U)^2 >} \tag{2}$$

The vertical profiles of turbulence τ/U are given in Figures 9 - 13. There are more cross channel variations in the turbulence profile. Since the velocities due to wave motion have not been separated from the total velocity, the plots show much larger turbulence levels in the presence of waves. The growth of the boundary layer as we move closer to the wavemaker can be clearly observed. The frequency spectra plots of the velocity are given in Appendix C. The spectra have been smoothed via Bartlett averaging. The spectra has 16 degrees of freedom and $\delta f = 0.02$ hz.

3 Monochromatic wave tests

The monochromatic wave tests have been divided into two parts - The breaking wave tests and the wave reflection tests. In both, the test cases consist of a range of wave heights for different wave periods. In the breaking wave tests the wave heights are larger, and most of the waves are breaking with very little wave reflection. In the wave reflection tests the incident wave heights are very small so that waves are reflected from the blocking point without any wave breaking.

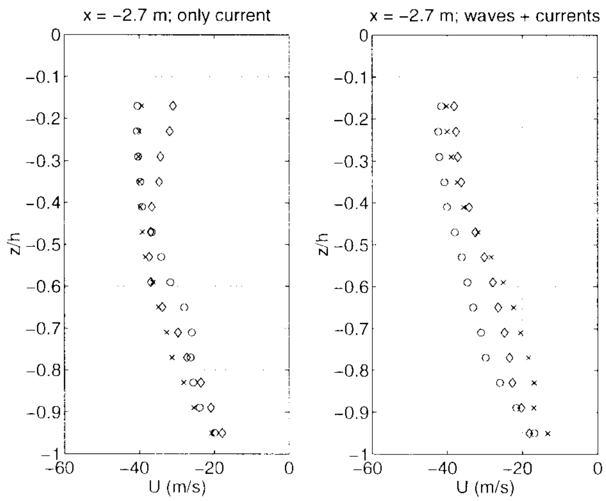

Figure 5: Mean velocity profiles at $x = -2.7$m;'$\circ$' $y/b = 0.25$,'$\times$' $y/b = 0.5$,'$\diamond$' $y/b = 0.75$

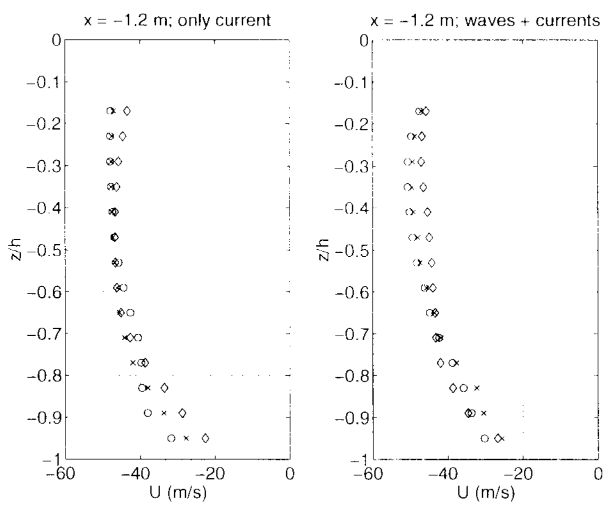

Figure 6: Mean velocity profiles at $x = -1.2$m;'$\circ$' $y/b = 0.28$,'$\times$' $y/b = 0.5$,'$\diamond$' $y/b = 0.72$

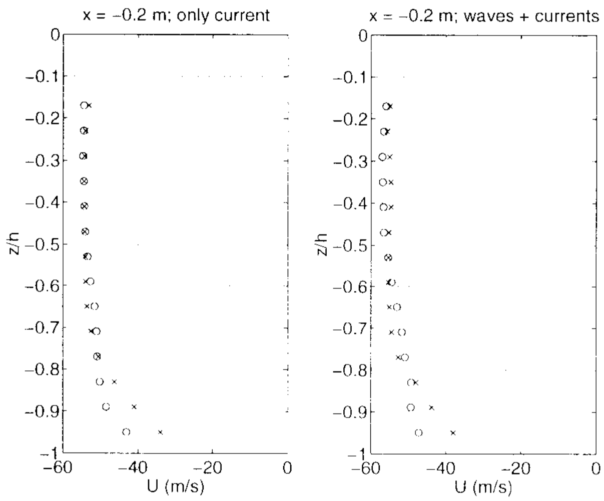

Figure 7: Mean velocity profiles at $x = -0.2$m;'∘' $y/b = 0.34$,'×' $y/b = 0.66$

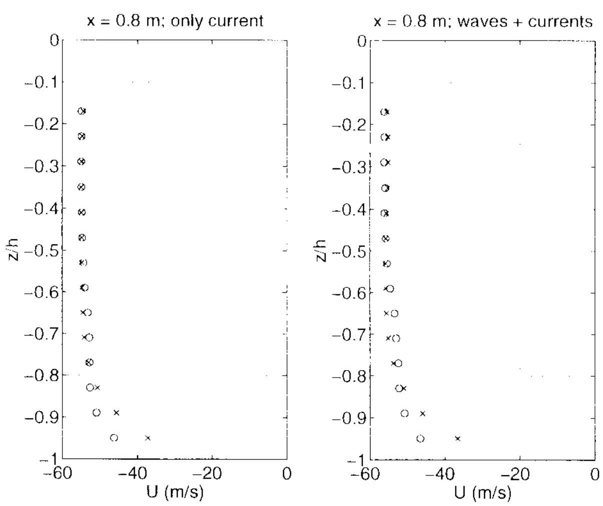

Figure 8: Mean velocity profiles at $x = 0.8$m;'∘' $y/b = 0.36$,'×' $y/b = 0.64$

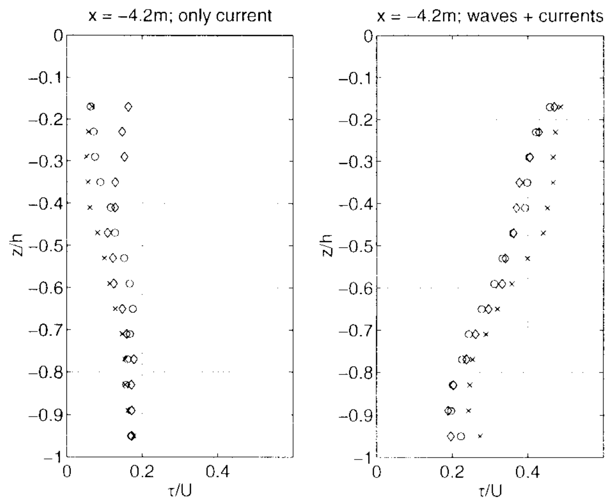

Figure 9: Turbulence profiles at $x = -4.2$m;'$\circ$' $y/b = 0.25$,'$\times$' $y/b = 0.5$,'$\diamond$' $y/b = 0.75$

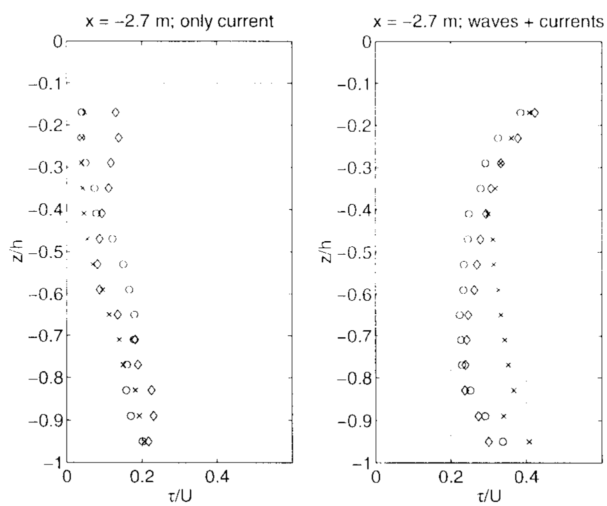

Figure 10: Turbulence profiles at $x = -2.7$m;'$\circ$' $y/b = 0.25$,'$\times$' $y/b = 0.5$,'$\diamond$' $y/b = 0.75$

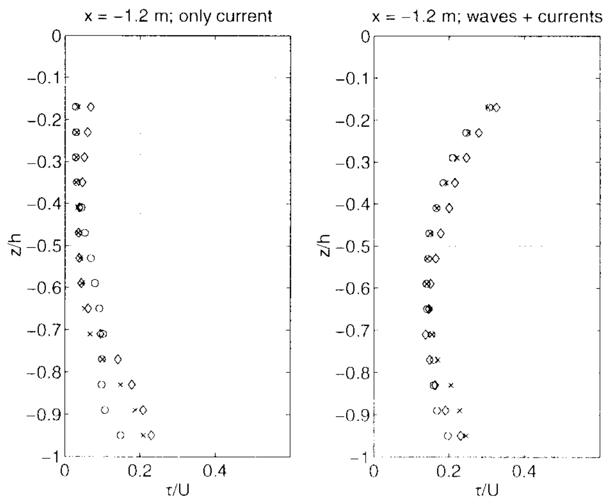

Figure 11: Turbulence profiles at $x = -1.2$m;'∘' $y/b = 0.28$,'×' $y/b = 0.5$,'⋄' $y/b = 0.72$

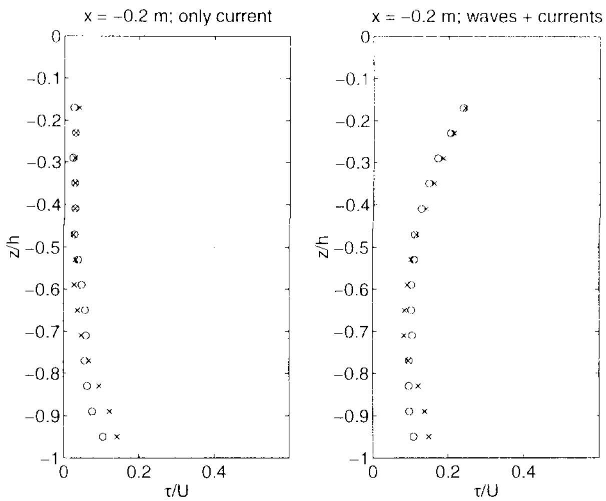

Figure 12: Turbulence profiles at $x = -0.2$m;'∘' $y/b = 0.34$,'×' $y/b = 0.66$

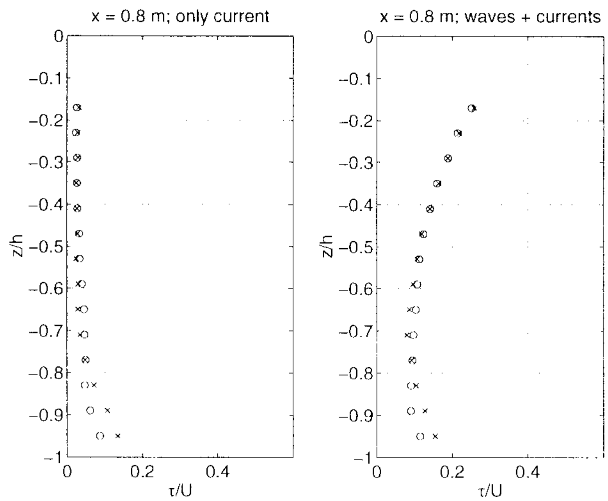

Figure 13: Turbulence profiles at $x = 0.8$m;'o' $y/b = 0.36$,'×' $y/b = 0.64$

3.1 Breaking wave tests

A total of 18 breaking wave test cases were run. The tests have been divided into 3 groups. Each group consists of 6 cases in which the wave period is kept constant and the wave height varied from small to large values. Data has been collected in the form of a time series of the water surface with the help of the capacitance wave gages. A total of 8 capacitance gages were used and data was recorded for 256 wave periods. For each test a detailed data set of 29 gage locations is obtained. This is done by keeping the first gage fixed and moving the remaining 7 gages to 4 different locations and repeating the experiments. The data set from the 4 different runs at the first gage (located at $x = -5.2$ m) is then used to determine the initial conditions (see Table 1) and also to test the repeatability of the experiments. Figure 14 shows the % deviation in the mean wave heights at the first gage, and shows that the experiments are fairly repeatable to within 6% error.

The wave height and wave period distributions for all the 18 tests are shown in Figures 16 and 17. From Table 1 we can see that Tests 1 to 6 have the same initial wave period with the wave height increasing from Test 1 to Test 6. The same hierarchy exists also for Tests 7 to 12 and Tests 13 to 18, but at different wave periods. The first two group of tests lie in the regime where the waves are blocked in the linear limit by the current. The last group of tests lie just above the linear blocking limit. Except for Tests

1, 7 and 13, where the wave amplitudes are very small, wave breaking due to strong opposing currents was observed in all the test cases. The shoaling of the waves as they propagate into the narrowing channel can be clearly observed, followed by the subsequent decay of wave energy in the narrow part of the channel due to wave breaking and blocking. Fluctuations in the water surface due to the turbulence in the current, are less than 1 cm and make up the noise in the system. Thus, when the wave amplitude falls to the order of these fluctuations, the wave period distribution becomes scattered.

In Tests 1 and 7, where the initial wave amplitude was very small, wave reflection from the blocking point was observed. In Test 13 the wave period is just above the minimum required wave period for wave blocking and we do not expect any waves to be blocked. However the scatter in the data suggests that there might be partial wave blocking (Stiassnie and Dagan, 1979), which disappears for the larger wave heights. The amplitude dispersion effects on the location of the blocking point can be clearly observed in the first group of tests as the wave amplitude increases from Test 1 to Test 6. Similar amplitude effects can also be observed in the Tests 7 to 12. From Figure 17 we find that the wave shifts to a longer period in Tests 5 and 6. This shift is due to the growth of side band instabilities and is the reason why the waves in these two test cases do not get blocked. These shifts also occur in Tests 9, 10, 11 an 12 but are not as prominent. In the last group of tests there are no significant effects of the side bands. The evolution of the side bands through the domain can be seen in the frequency spectra plots for the monochromatic tests (see Appendix D). The frequency spectra have been plotted on a semilog scale. For each case the frequency spectra have been smoothed via Bartlett averaging, giving 12 degrees of freedom and $\delta f \approx 0.012$ hz.

3.2 Wave reflection tests

Wave reflection from the blocking point occurs only when the incident wave is small enough such that there is no wave breaking at or before the blocking point. Since wave energy cannot propagate beyond the blocking point, and no energy is lost due to wave breaking, the waves get reflected back. The reflected waves are peculiar in the sense that their phase speed is still moving against the current, but their group velocity moves with the current. In other words the wave energy is washed down by the currents. As the waves propagate further away from the blocking region, they continue to get shorter and shorter. The incident and reflected waves superimpose to form the typical nodes and antinodes patterns in the amplitude envelope.

To study this phenomenon a total of 15 test cases were run. Just like in the wave breaking experiment, the tests were divided into three groups. Each group consisted of 5 test cases having a constant wave period and increasing wave heights. The incident wave heights were gradually increased to study the effects of nonlinearity on the shape of the amplitude envelope. Wave blocking occurred close to the narrowest part of the channel ($x = 0$). To capture the variation in the amplitude shape close to the blocking region, 43 gage measurements were made between $x = -1.5$ m and $x = 0.8$ m. At each gage location the time series have been recorded for 256 wave periods. Similar to the breaking wave tests a detailed data set was obtained by moving the gages to different locations and repeating the experiments. This was done 6 times. The initial conditions were obtained from a fixed gage kept at $x = -4.6$ m, and is tabulated in Table 2. The repeatability tests (Figure 15) show that the experiments are repeatable to within 4% error.

Wave height and period distributions for all the 15 test cases are shown in Figures 18 and 19. Scatter in the wave period distribution, at low wave amplitudes occurs due to the noise in the system. Apart from this scatter, the wave period remains constant for all the test cases. This is because the wave heights are too small to develop any side band instabilities. The change in the shape of the amplitude envelope, with increasing wave amplitude, is clearly visible when we move from Test 1 to 5, and then again for Tests 6 to 10 and Tests 11 to 15. In the case of Test 11, according to linear theory, no blocking should occur. But partial wave reflection still occurs because the required blocking current is close to the maximum current (Stiassnie and Dagan, 1979). With increasing amplitude, the required blocking current moves further away from the maximum current, and no wave reflection pattern is observed. The frequency spectra for all the test cases are shown in Appendix E. The frequency spectra have been plotted on a semilog scale. For each case the frequency spectra have been smoothed via Bartlett averaging, giving 12 degrees of freedom and $\delta f \approx 0.012$ hz.

Table 1: Parameters for monochromatic breaking wave tests determined at $x = -5.2$ m

Test No.	T (s)	H (m)	Sampling freq (Hz)
1	1.2	0.012	83.333
2	1.2	0.018	83.333
3	1.2	0.033	83.333
4	1.2	0.066	83.333
5	1.2	0.095	83.333
6	1.2	0.126	83.333
7	1.3	0.014	76.923
8	1.3	0.029	76.923
9	1.3	0.057	76.923
10	1.3	0.084	76.923
11	1.3	0.104	76.923
12	1.3	0.130	76.923
13	1.4	0.016	71.429
14	1.4	0.026	71.429
15	1.4	0.071	71.429
16	1.4	0.096	71.429
17	1.4	0.117	71.429
18	1.4	0.141	71.429

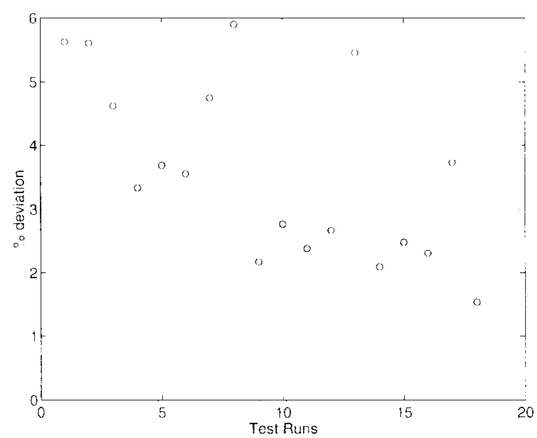

Figure 14: Repeatability for monochromatic breaking wave tests

Table 2: Parameters for monochromatic wave reflection tests determined at $x = -4.6$ m

Test No.	T (s)	H (m)	Sampling freq (Hz)
1	1.2	0.012	83.333
2	1.2	0.013	83.333
3	1.2	0.014	83.333
4	1.2	0.015	83.333
5	1.2	0.016	83.333
6	1.2	0.013	83.333
7	1.3	0.015	76.923
8	1.3	0.018	76.923
9	1.3	0.021	76.923
10	1.3	0.024	76.923
11	1.3	0.015	76.923
12	1.3	0.020	76.923
13	1.4	0.025	71.429
14	1.4	0.032	71.429
15	1.4	0.038	71.429

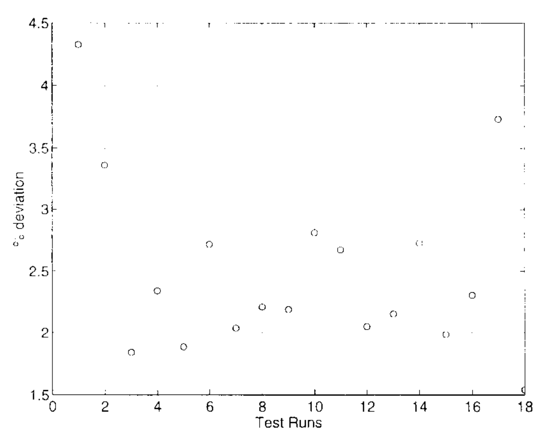

Figure 15: Repeatability for monochromatic wave reflection tests

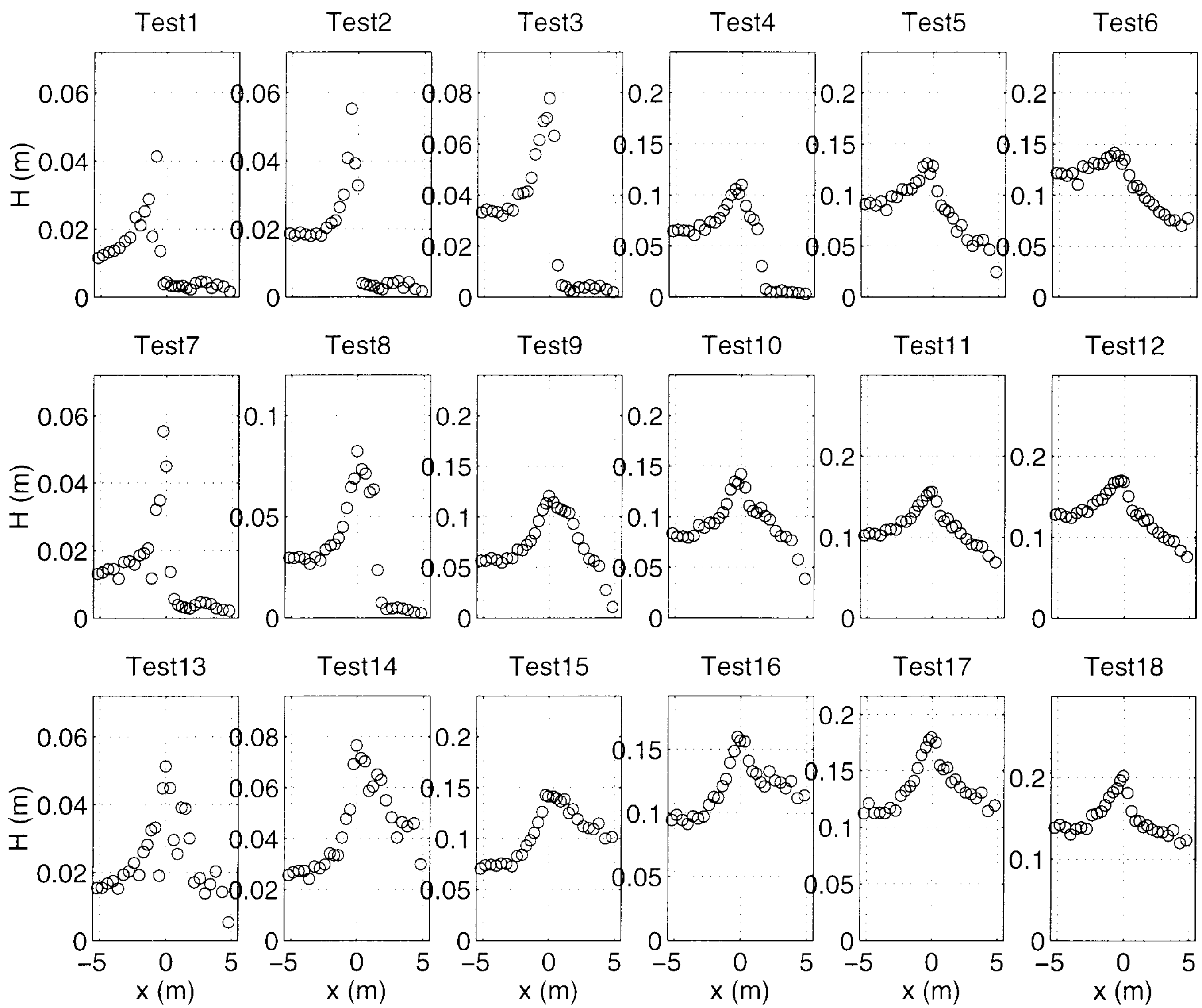

Figure 16: Wave height distribution for monochromatic breaking wave tests

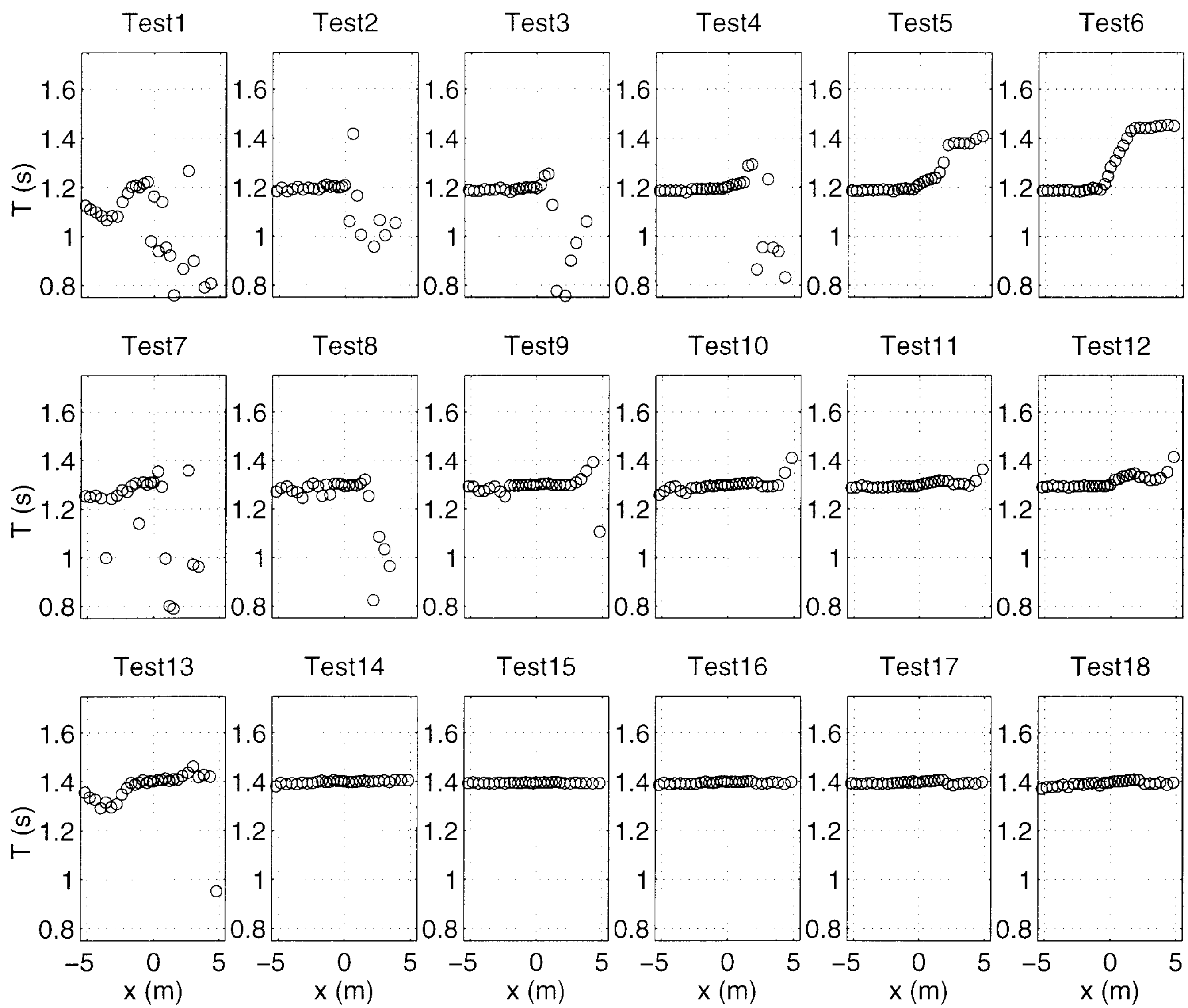

Figure 17: Wave period distribution for monochromatic breaking wave tests

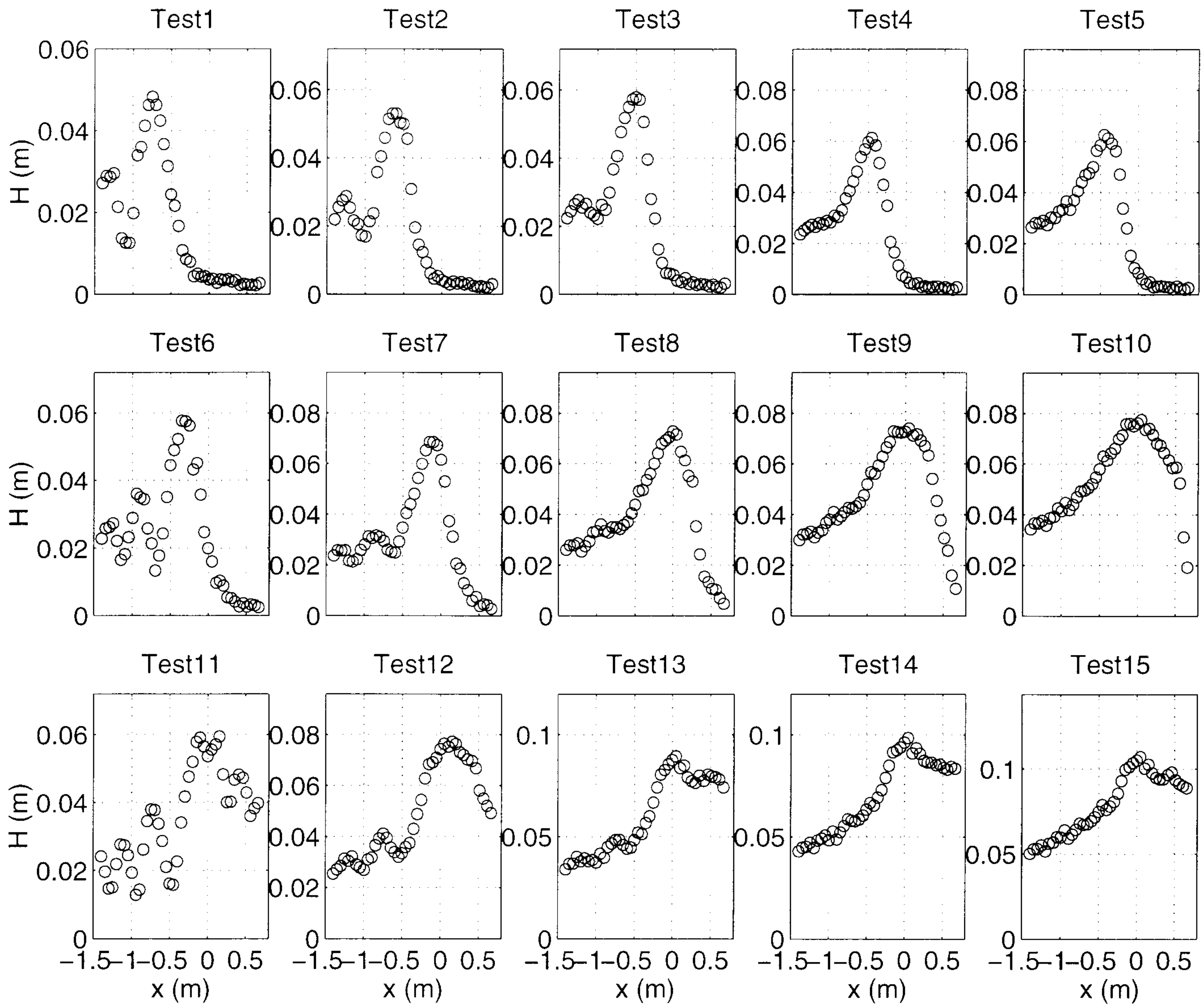

Figure 18: Wave height distribution for monochromatic wave reflection tests

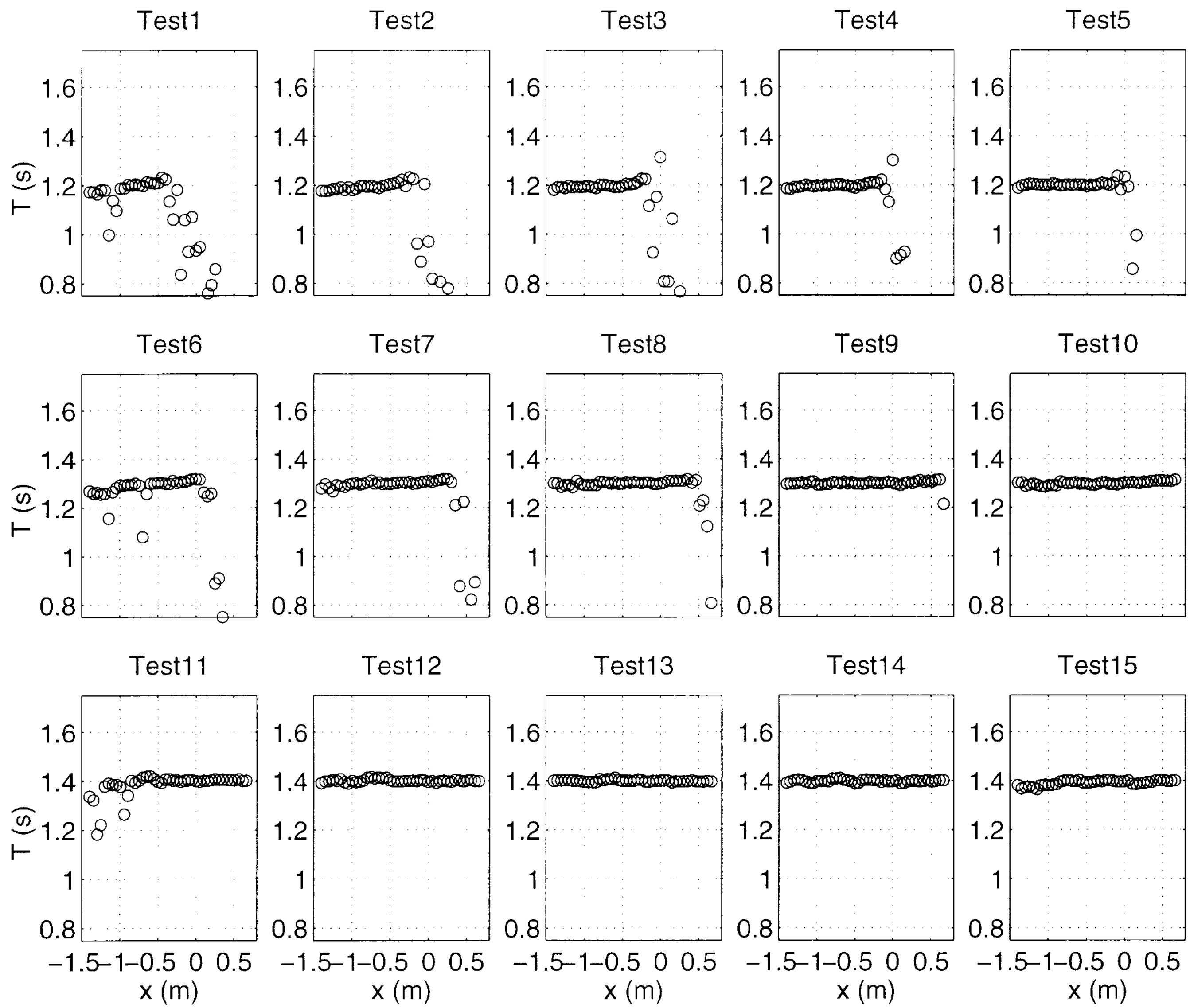

Figure 19: Wave period distribution for monochromatic wave reflection tests

4 Random wave tests

The motivation for conducting random wave tests was to study the dynamics of the wave field under blocking and current limited breaking conditions. To do this 20 spectral design conditions were used. The aim was to use TMA spectra for all our cases, but this was not possible because, due to the strong current, all the high frequency components were blocked at the paddle itself. The experiments were initially designed such that there were 5 groups of 4 test cases. In each group the peak frequency was kept fixed and the energy of the spectrum varied. But, the spectrum evolves as it moves against the current, and the spectrum measured at the first gage showed that the peak frequency shifted depending upon the wave energy of the spectrum. As a result, the initial spectral quantities for our experiments were determined from the first gage which was fixed at $x = -4.6$ m. The results are shown in Table 3 in terms of the significant wave height (H_s) and significant wave period (T_s), determined with the help of a zero-upcrossing method. The initial test spectra are also shown in Figures 21 and 22.

For each test case, 36 gage measurements were made between $x = -4.6$ m and $x = 4.61$ m. The detailed measurement set was obtained by moving the gages and repeating the experiments 5 times. Figure 20 shows that the experiments were repeatable to within 3% for all the test cases. The record length at each gage was 1000 seconds, and sampling frequency was fixed at 50 hz. The significant wave heights and periods were obtained with the help of the zero-upcrossing method, and are shown in Figures 23 to 26. The tests vary from most of the spectrum getting blocked, to almost no blocking. In all the tests wave breaking was observed. The frequency spectra plots for all the test cases are given in Appendix F. The spectra have been smoothed using a Bartlett averaging technique, giving 24 degrees of freedom and $\delta f = 0.012$.

Table 3: Spectral parameters for random wave tests determined at $x = -4.6$ m

Test No.	T_s (s)	H_s (m)
1	1.09	0.037
2	1.12	0.047
3	1.17	0.06
4	1.19	0.066
5	1.18	0.035
6	1.2	0.048
7	1.24	0.066
8	1.25	0.082
9	1.25	0.045
10	1.27	0.066
11	1.3	0.084
12	1.31	0.099
13	1.3	0.043
14	1.32	0.061
15	1.33	0.08
16	1.36	0.098
17	1.37	0.036
18	1.42	0.054
19	1.46	0.071
20	1.47	0.086

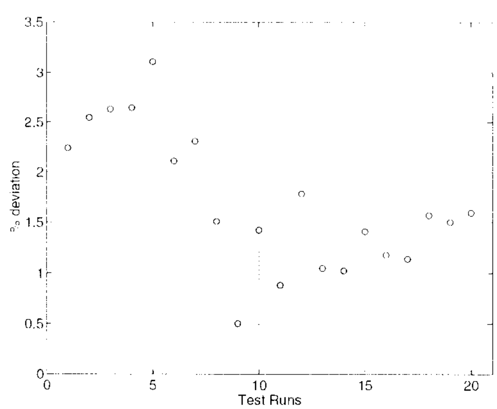

Figure 20: Repeatability for random wave tests

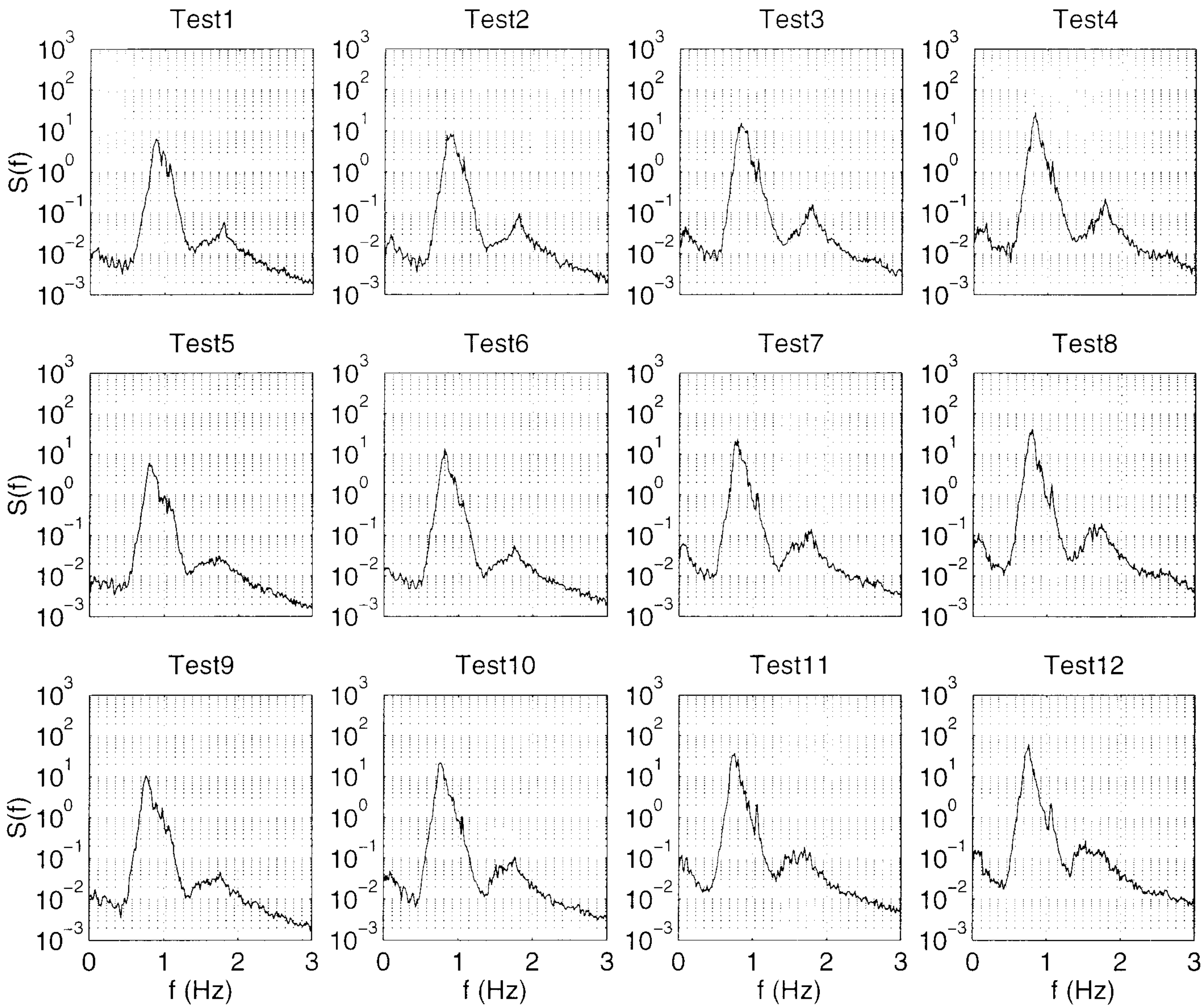

Figure 21: Incident frequency spectra for random wave tests 1 – 12, measured at $x = -4.6$ m

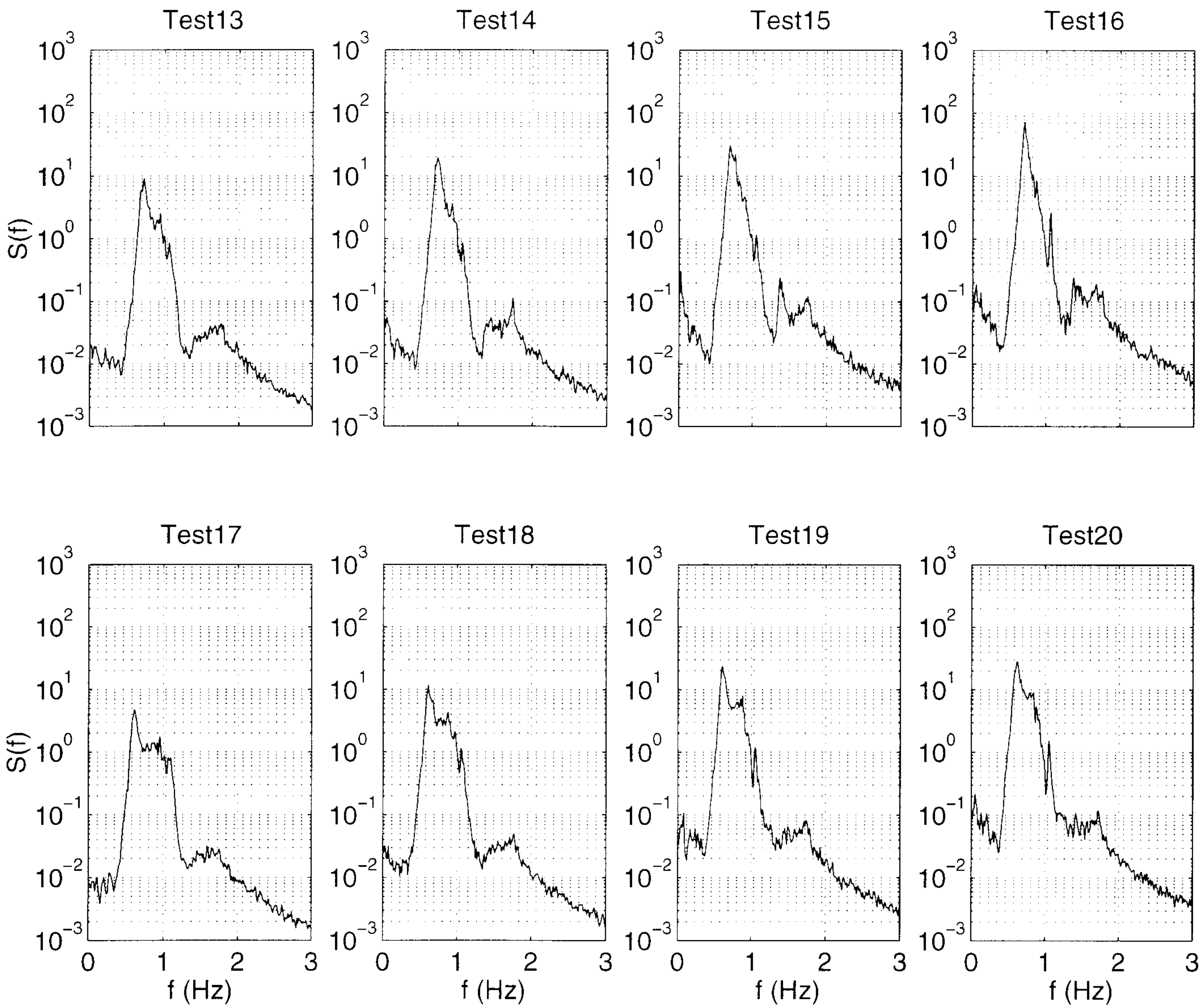

Figure 22: Incident frequency spectra for random wave tests 13 – 20, measured at $x = -4.6$ m

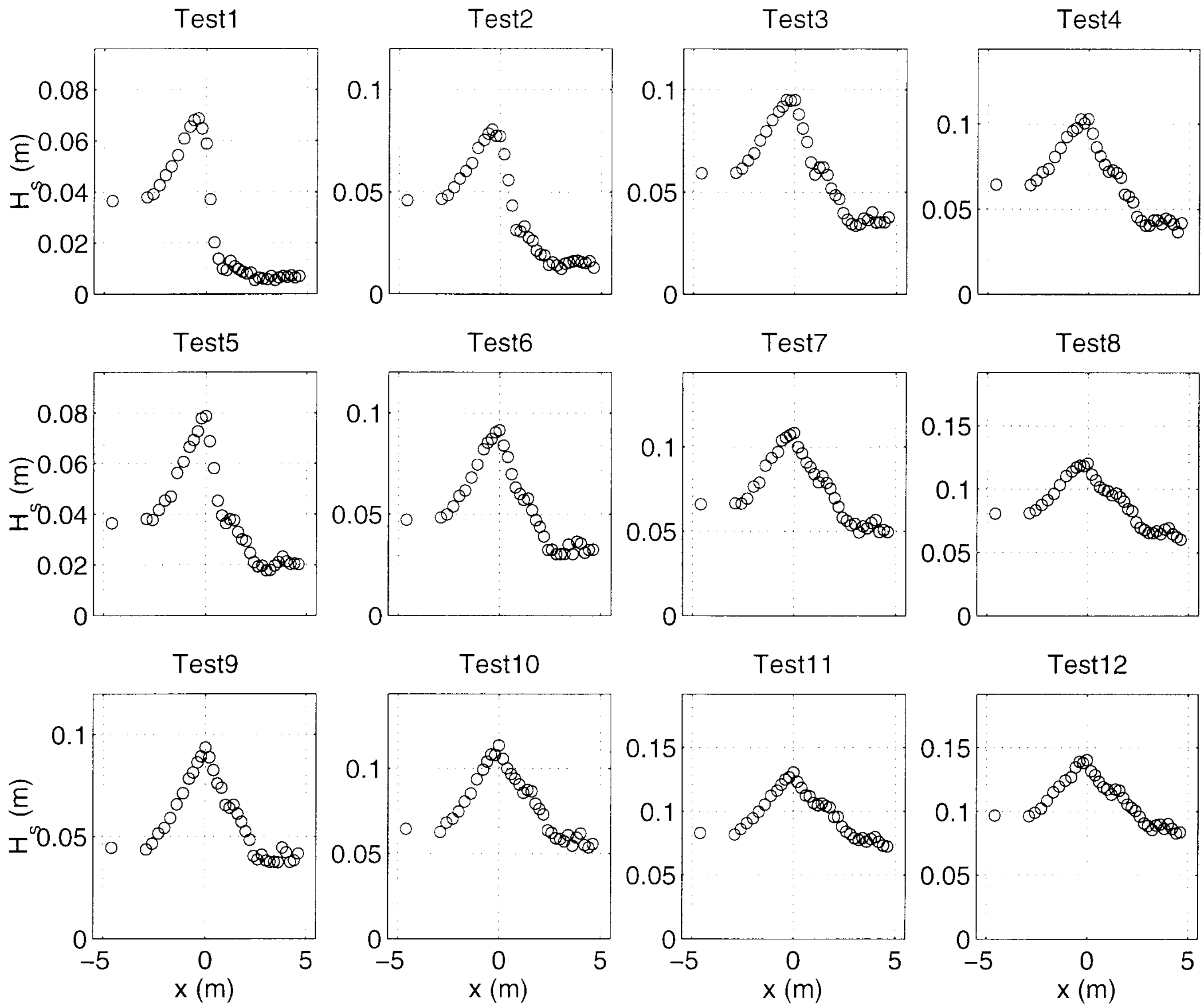

Figure 23: Significant wave height distribution for random wave tests 1 – 12

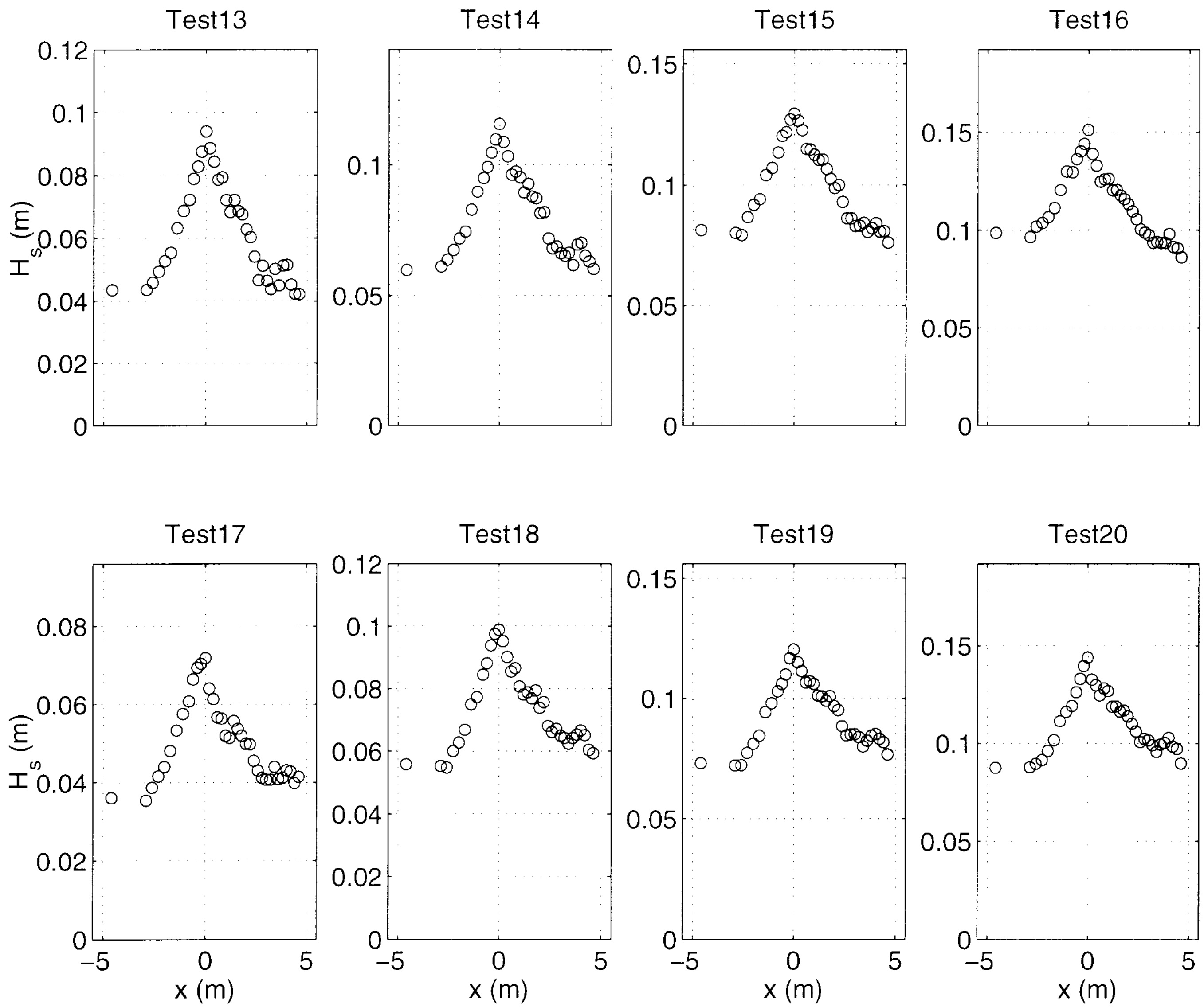

Figure 24: Significant wave height distribution for random wave tests 13 − 20

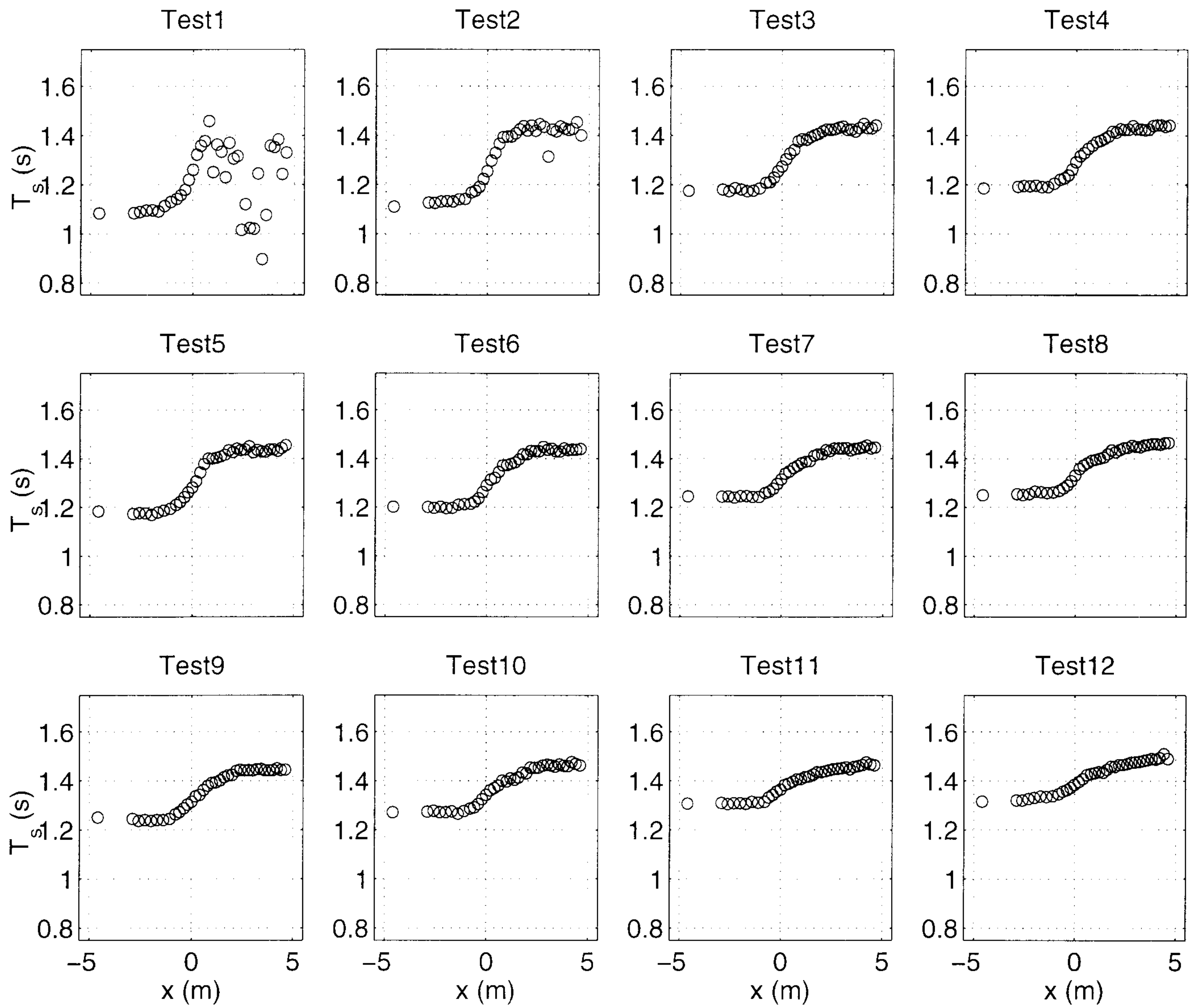

Figure 25: Significant wave period distribution for random wave tests $1 - 12$

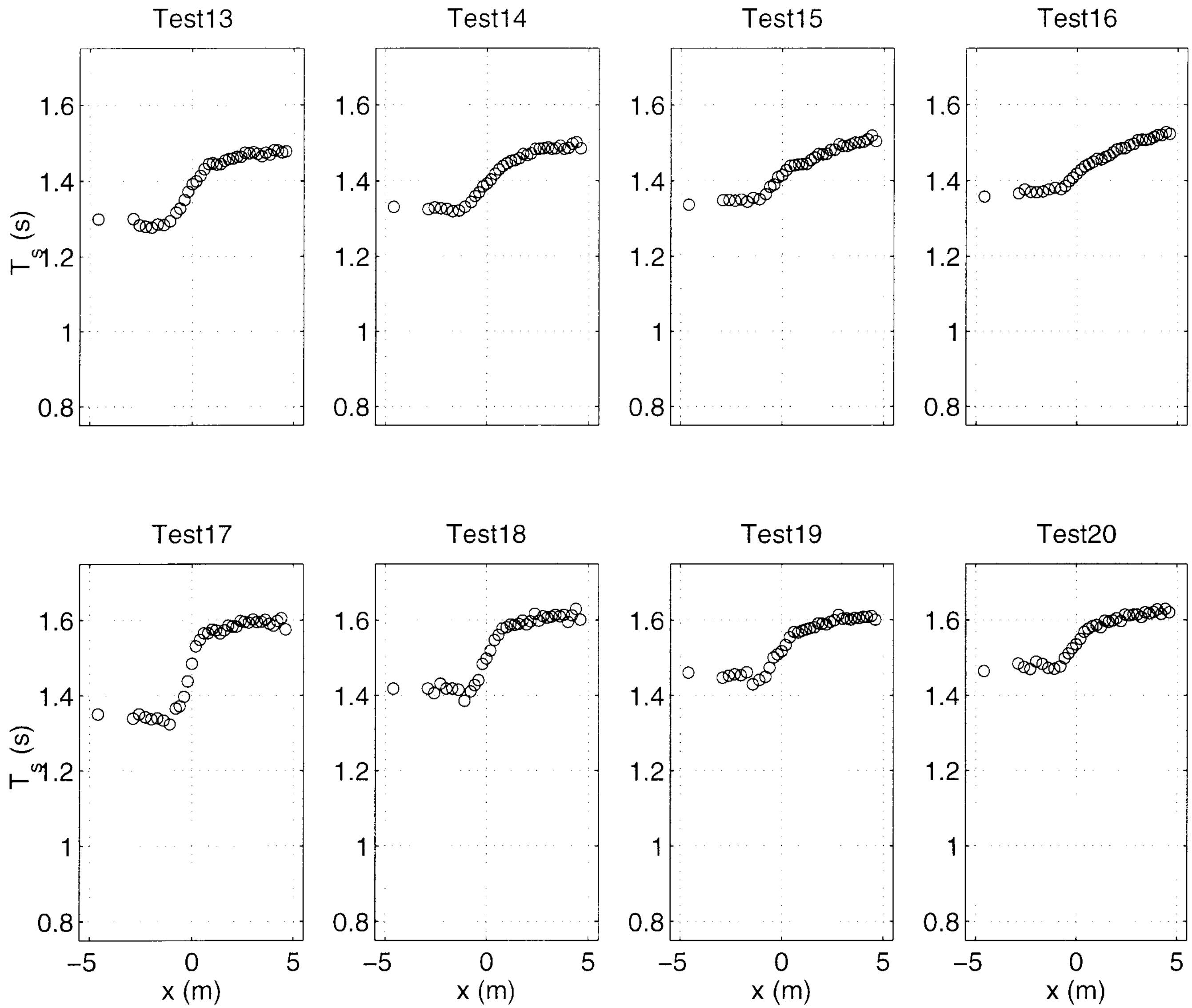

Figure 26: Significant wave period distribution for random wave tests 13 – 20

5 Narrow banded wave spectra

Experiments were also conducted with narrow banded wave spectra. These tests were divided into two parts -- Wave groups (obtained from a bichromatic spectrum) and wave packets (obtained from a normally distributed spectrum). The aim was to see the effects of a moving blocking point due to a modulating wave train.

5.1 Wave group tests

Wave groups were constructed by superposing two monochromatic waves having the same amplitude but slightly different frequencies. The difference between the frequencies determining the number of waves in a group. In all 3 different sets of wave groups were used. Each set consisted of 4 different energy levels, making a total of 12 tests. The test particulars are given in Table 4. Similar to the random wave tests, 36 gage measurements were made for each test between $x = -4.6$ m and $x = 4.61$ m, by moving the gages and repeating the experiments 5 times. Figure 27 shows that the experiments were repeatable to within 3% for all the test cases.

The frequency spectra at the first gage ($x = -4.6$ m) for all the test cases are shown in Figure 28. From the figure it is obvious that the initial spectra is not bichromatic. For the larger wave amplitude tests, wave energy is transferred to the side bands. There is also an extra wave component at a frequency slightly greater than 1 hz. The closer the frequency of one of the design wave components to 1 hz, the greater is the energy at this undesired wave component. The cause for this anomalous behavior is currently being studied. The corresponding time series for these tests are shown in Figures 29 and 30. The evolution of the frequency spectra and corresponding time series for all the tests is given in Appendices I and J.

5.2 Wave packet tests

Wave packets have been generated with the help of Gaussian shaped frequency spectra. For our experiments 12 design test conditions were generated. Just like in the case of the wave group tests, these tests have been divided into 3 sets. Each set consisting of 4 different test conditions with

Table 4: Parameters for wave group tests determined at $x = -4.6$ m

Test No.	T_1 (s)	T_2 (s)	H_s (m)	Sampling freq (hz)
1	1.06	1.2	0.028	88.889
2	1.06	1.2	0.054	88.889
3	1.01	1.3	0.028	87.912
4	1.01	1.3	0.054	87.912
5	1.15	1.3	0.025	82.051
6	1.15	1.3	0.053	82.051
7	1.06	1.2	0.068	88.889
8	1.06	1.2	0.098	88.889
9	1.01	1.3	0.068	87.912
10	1.01	1.3	0.083	87.912
11	1.15	1.3	0.074	82.051
12	1.15	1.3	0.089	82.051

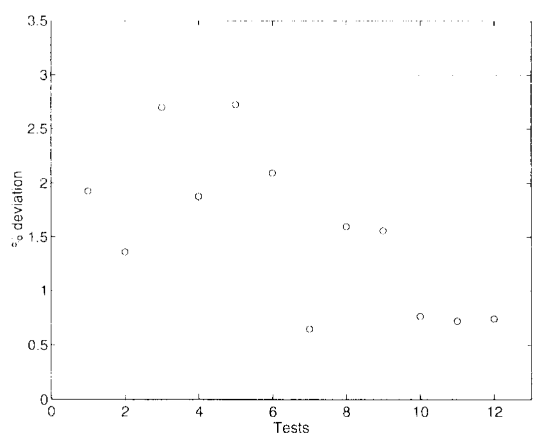

Figure 27: Repeatability for wave group tests

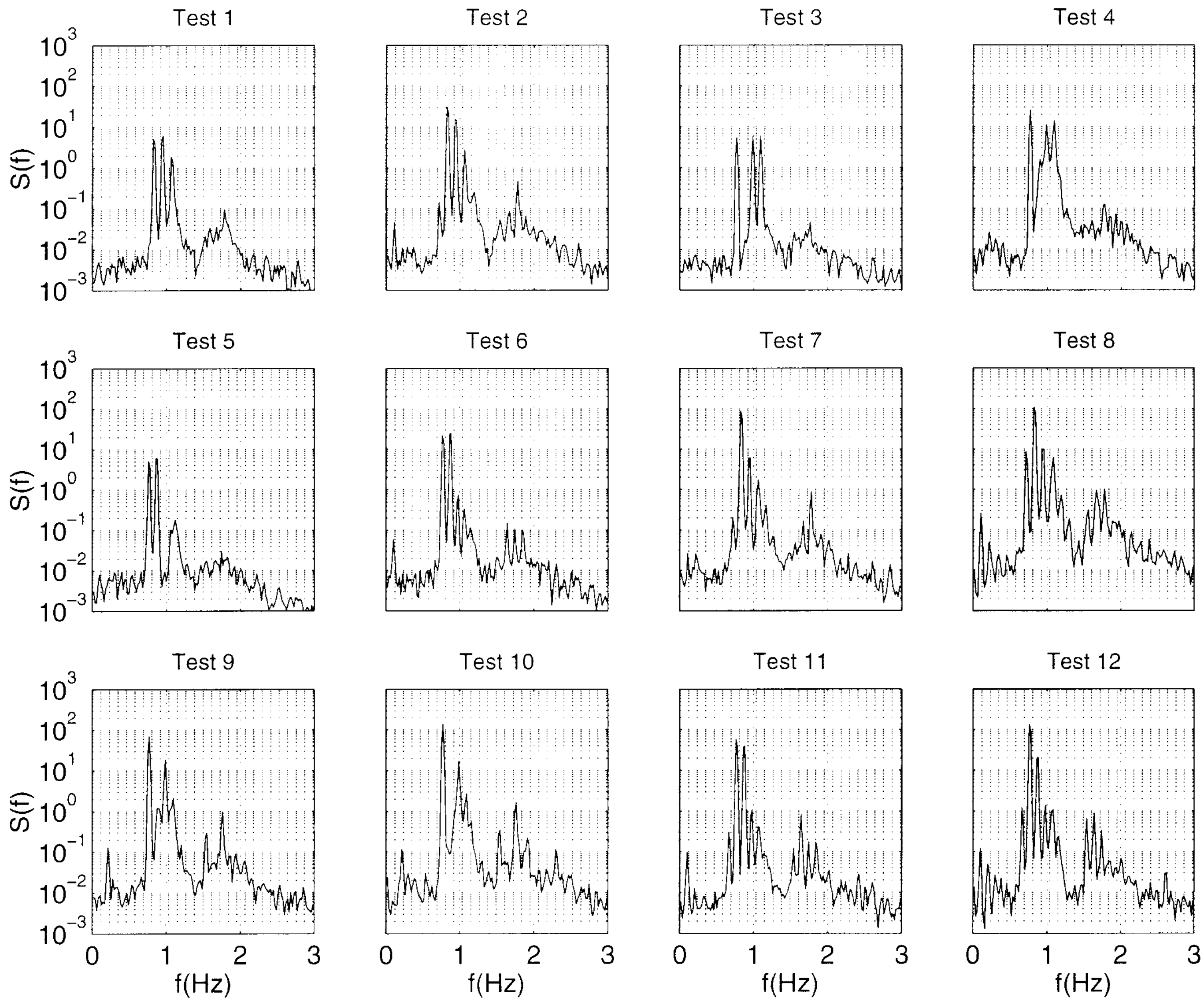

Figure 28: Frequency spectra at $x = -4.6$ m for wave group tests

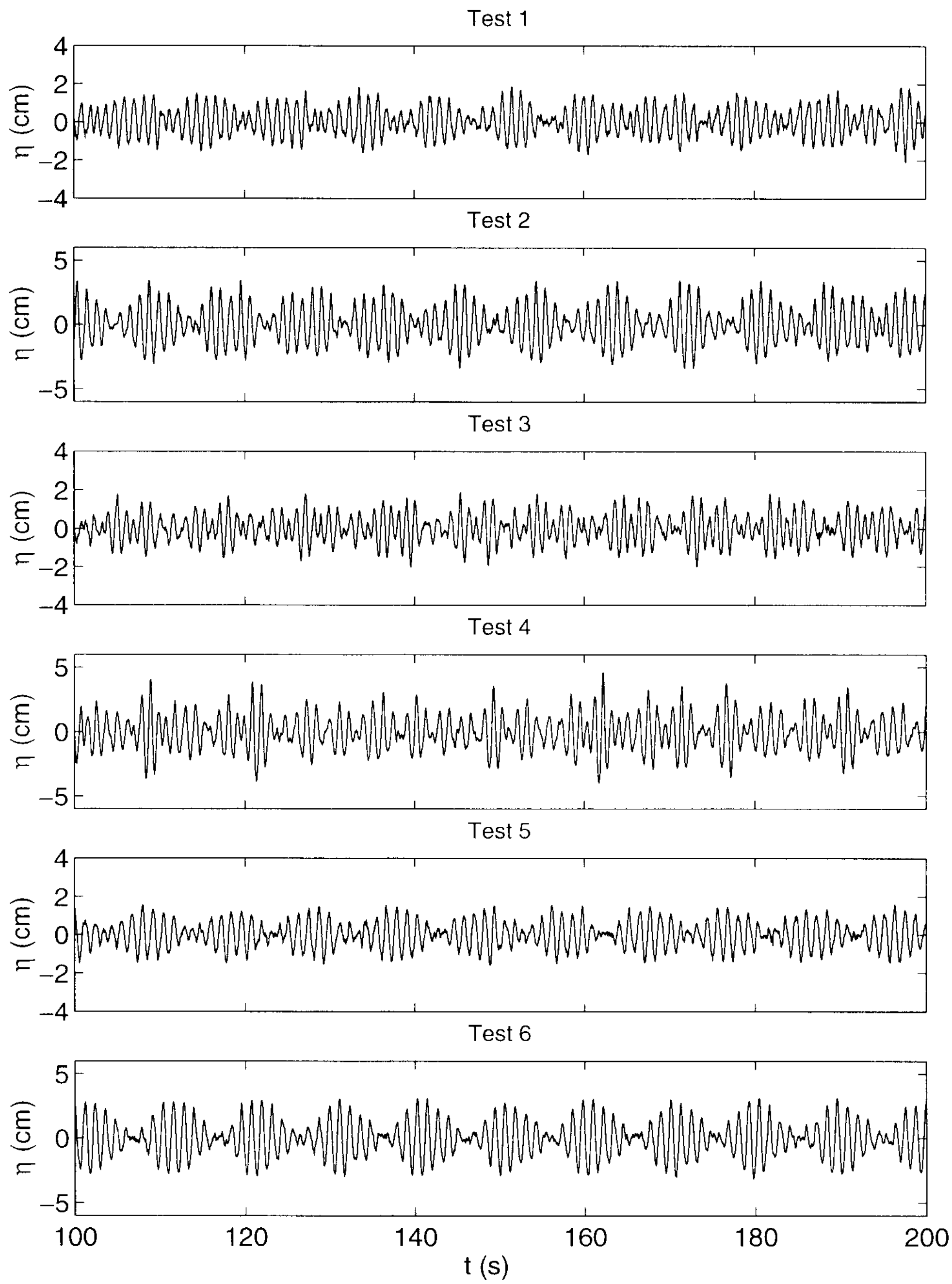

Figure 29: Time series at $x = -4.6$ m for Tests 1 – 6 (wave group tests)

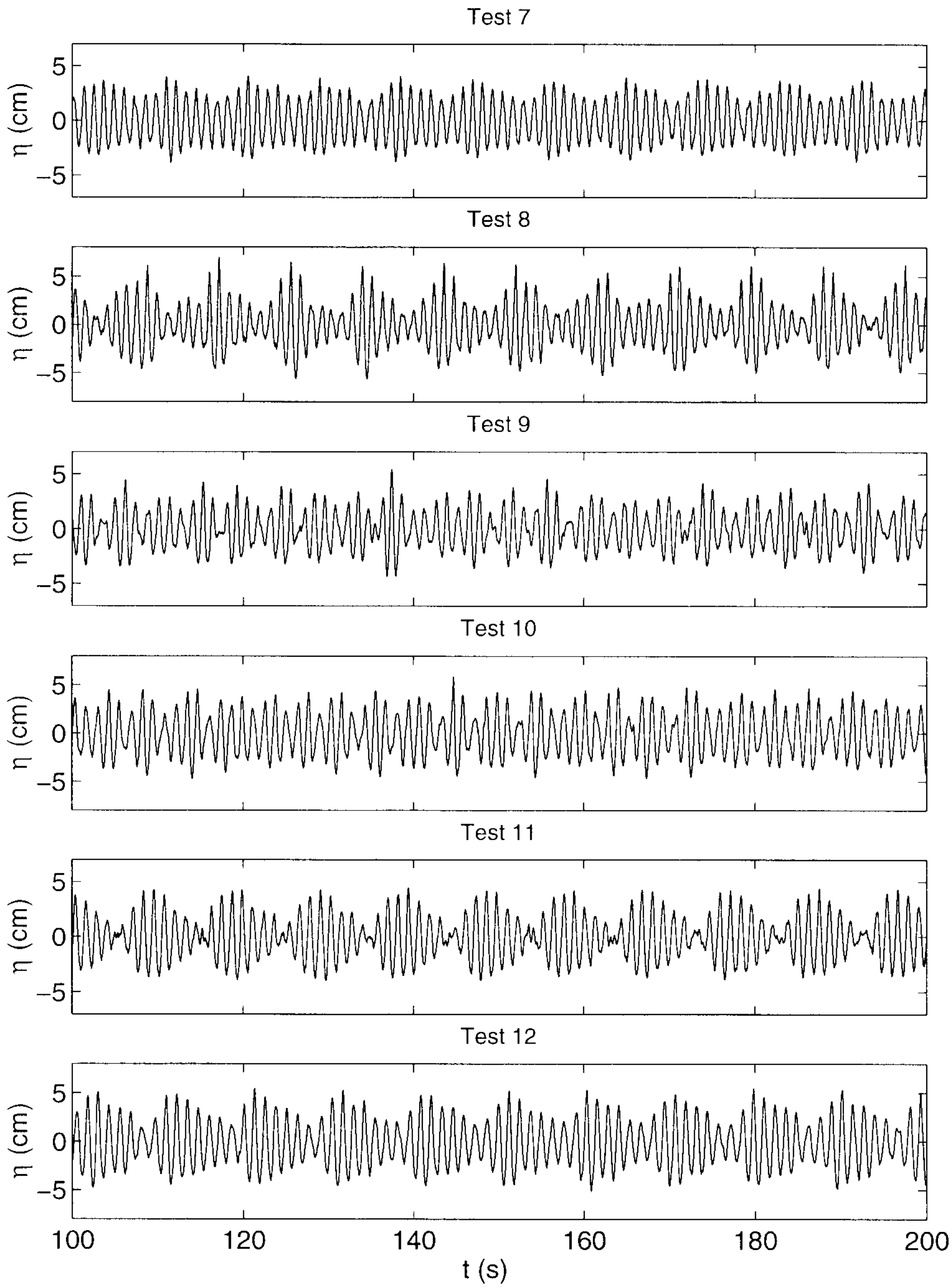

Figure 30: Time series at $x = -4.6$ m for Tests $7 - 12$ (wave group tests)

Table 5: Parameters for wave packet tests determined at $x = -4.6$ m

Test No.	T_p (s)	H_{max} (m)	α
1	1.125	0.0175	0.08
2	1.125	0.035	0.08
3	1.137	0.013	0.15
4	1.137	0.02	0.15
5	1.219	0.017	0.08
6	1.219	0.032	0.08
7	1.125	0.07	0.08
8	1.125	0.094	0.08
9	1.137	0.031	0.15
10	1.137	0.05	0.15
11	1.219	0.054	0.08
12	1.219	0.084	0.08

varying energy content. The equation for the design spectra was given by

$$S(f) = \frac{\gamma}{\sqrt{2\pi}\alpha} \exp(-0.5\frac{(f - f_p)^2}{\alpha^2}) \tag{3}$$

where, f_p is the peak frequency, and γ and α are coefficients determining the energy content and width of the spectrum. The larger the value of α, the lesser the number of individual wave components in the packet.

The time series of the wave paddle motion for the 12 cases are shown in Figures 31 and 32. Unfortunately, by the time the wave packet reached the first gage ($x = -4.6$ m), the packet had diffused out, leading to much smaller wave heights (see Figures 33 and 34). This is specially true for Test 3, where the signature of the wave packet has been all but lost in the noise of the water surface. The test particulars for the wave packet tests are given in Table 5. H_{max} is the maximum wave height in the wave packet. T_p is the peak period and α is the parameter used in (3). The modulation of the wave packets as they travel through the blocking region, and their corresponding frequency spectra are given in Appendices K and L. The sampling frequency for all the tests is 100 hz.

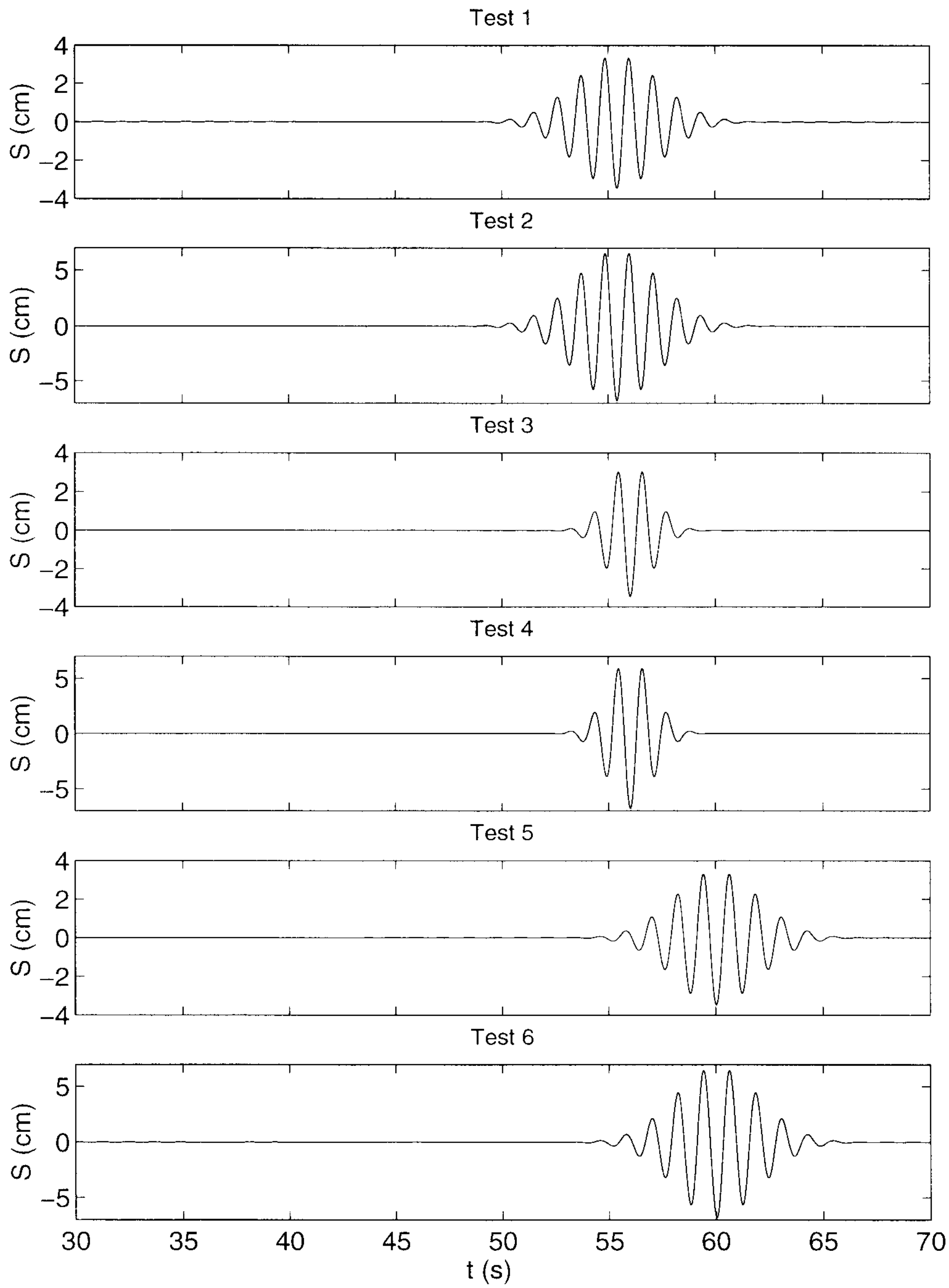

Figure 31: Time series of the wave paddle motion for Tests 1−6 (wave packet tests)

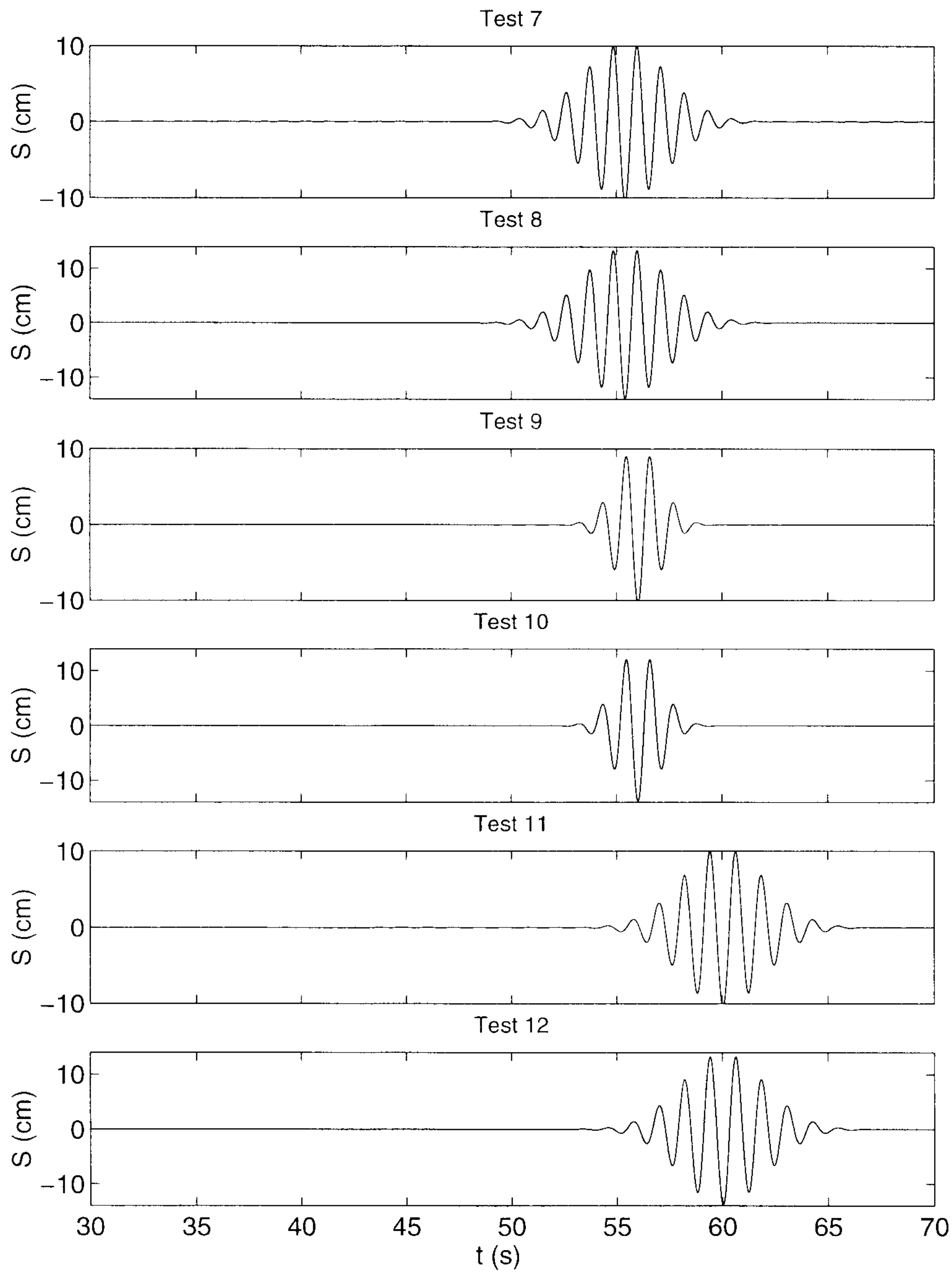

Figure 32: Time series of the wave paddle motion for Tests 7 – 12 (wave packet tests)

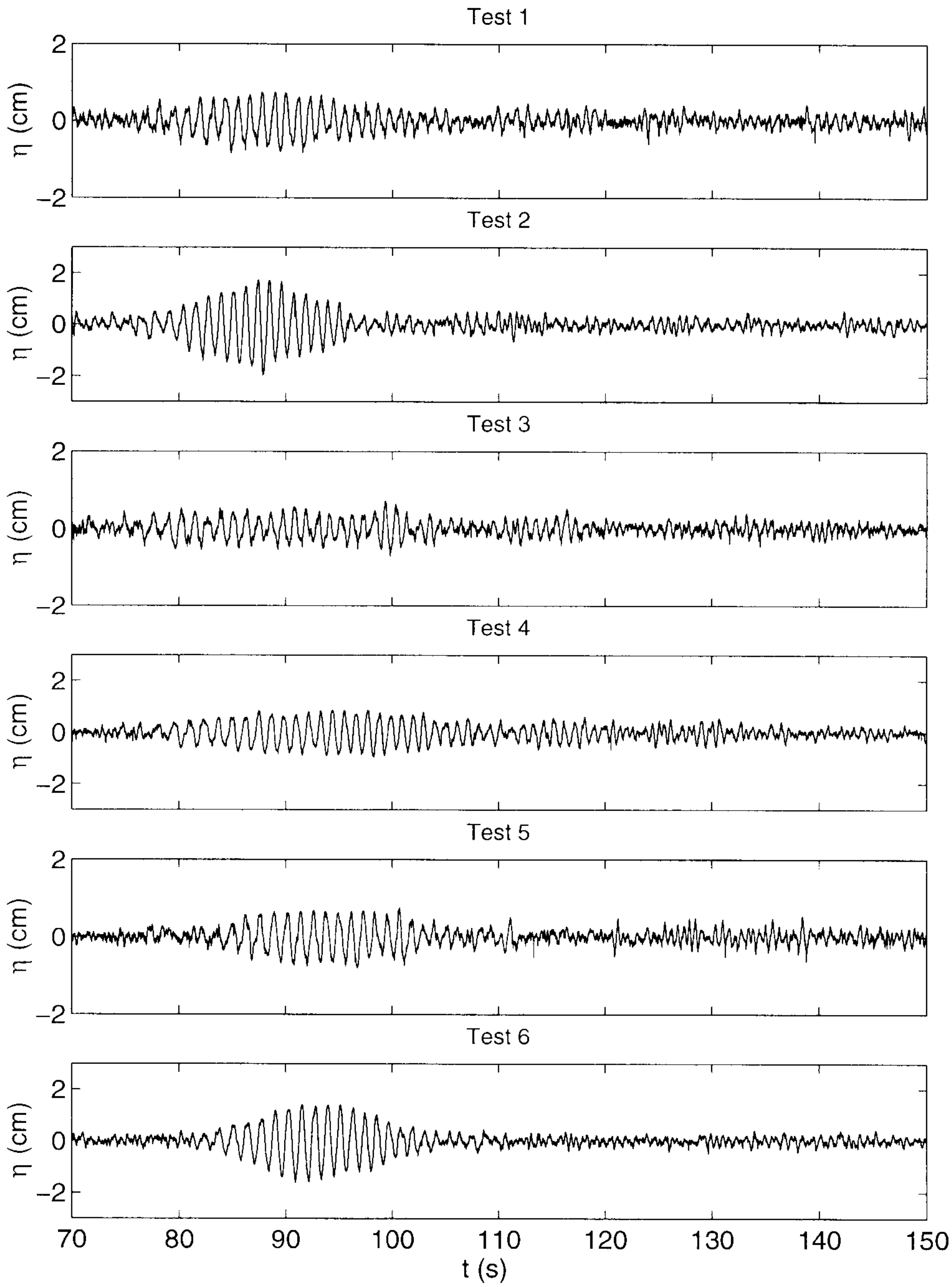

Figure 33: Time series of the water surface at $x = -4.6$ m for Tests 1 – 6 (wave packet tests)

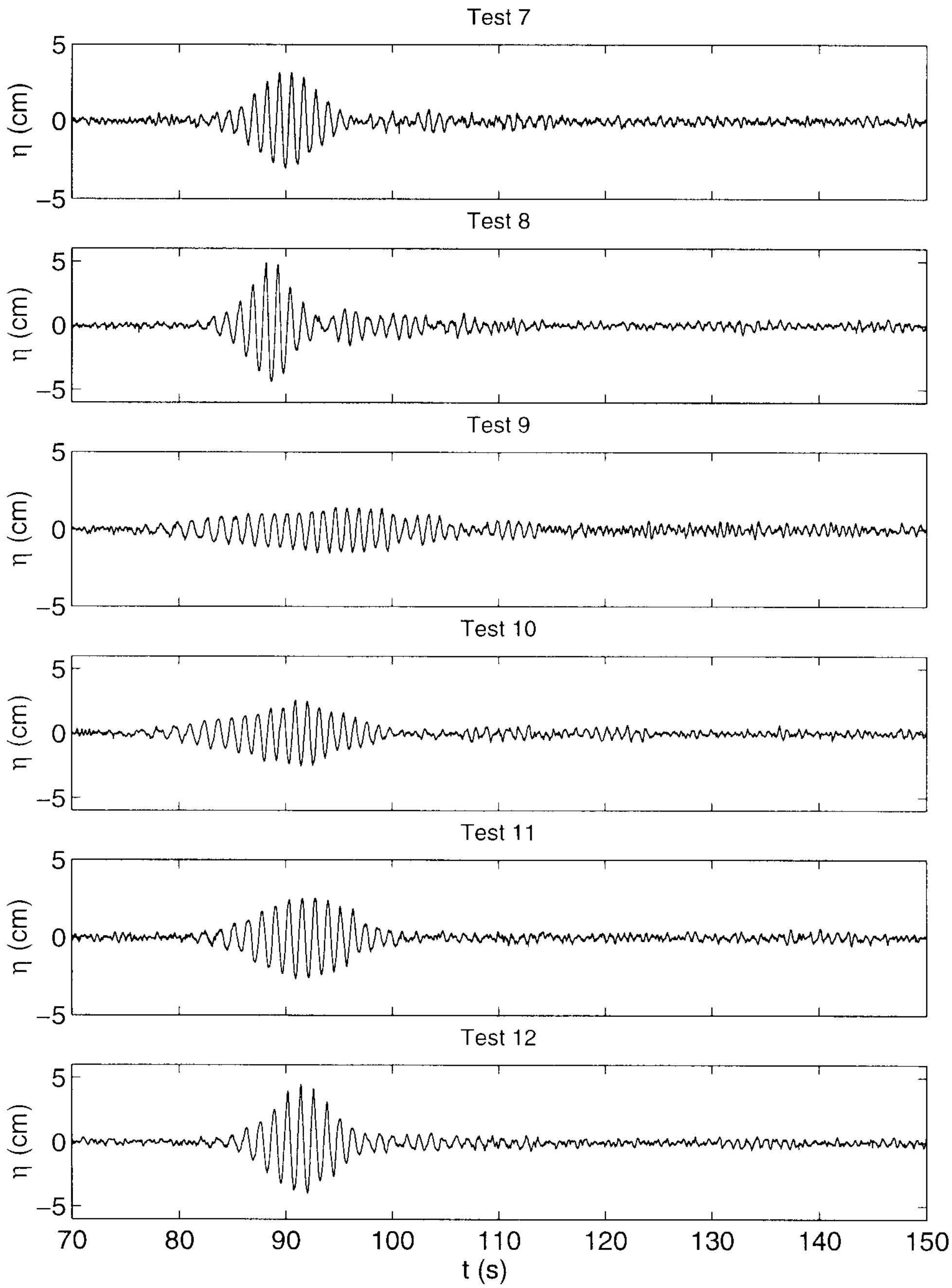

Figure 34: Time series of the water surface at $x = -4.6$ m for Tests 7 – 12 (wave packet tests)

Acknowledgments

This research has been sponsored by the U.S. Army Corps of Engineers, Coastal Engineering Research Center (Contract No. DACW 39-90-D-0006-D002) and by NOAA Office of Sea Grant, Department of Commerce, under Grant No. NA56RG0147 (Project No. R/OE-21). The U.S. Government is authorized to produce and distribute reprints for governmental purposes, not withstanding any copyright notation that may appear heron.

References

Bretherton, F. P. and Garrett, C. J. R. (1969). Wavetrains in inhomogenous moving media. *Proc. Roy. Soc. London A.*, **302**, 529–554.

Lai, R. J., Long, S. R., and Huang, N. E. (1989). Laboratory studies of wave-current interaction:kinematics of the strong interaction. *J. Geophys. Res.*, **94**(C11), 16201–16214.

Peregrine, D. H. (1976). Interaction of water waves and currents. *Advanced Applied Mechanics*, **16**, 9–117.

Shyu, J. H. and Phillips, O. M. (1990). The blockage of gravity and capillary waves by longer waves and currents. *J. Fluid Mech.*, **217**, 115–141.

Smith, R. (1975). Reflection of short gravity waves on a non-uniform current. *Math. Proc. Camb. Phil. Soc.*, **78**, 517–525.

Stiassnie, M. and Dagan, G. (1979). Partial reflexion of water waves by non-uniform adverse currents. *J. Fluid Mech.*, **92**(1), 119–129.

Trulsen, K. and Mei, C. C. (1993). Double reflection of capillary/gravity waves by a non-uniform current: a boundary-layer theory. *J. Fluid Mech.*, **251**, 239–271.

A Naming convention used for the data files

Both the ADV and the wave gage data have been stored in an ASCII format. The wave gage data is stored as a time series of the water surface in cm. The ADV data is stored as a time series of the velocity in cm/s.

The naming convention for the wave gage data for the different experiments is based on the dates on which the experiments were started and is given by

g[*gage no*]**_c.**[*date*]**t**[*test no*]

where, [*gage no*] signifies the gage location, [*test no*] the test and [*date*] the particular set of experiments.

Monochromatic breaking wave tests These experiments are denoted by *date = may15*. There are 18 different tests and each test consists of 29 gage measurements.

Monochromatic wave reflection tests These experiments are denoted by *date = aug30*. There are 15 different tests and each test consists of 43 gage measurements.

Wave group tests These experiments are denoted by *date = sep18*. There are 12 different tests and each test consists of 36 gage measurements.

Wave packet tests These experiments are denoted by *date = sep26*. There are 12 different tests and each test consists of 36 gage measurements.

Random wave tests These experiments are denoted by *date = oct09*. There are 20 different tests and each test consists of 36 gage measurements.

The ADV data measurements were made in the form of vertical profiles of the horizontal current. The naming convention for the ADV data is as follows

JUL[*pos no*]**S**[*prof no*]**.VEL**

where [*pos no*] denotes the vertical position of the measurement in a profile, and [*prof no*] denotes the particular profile. There are a total of 26 profile measurements and their particulars are given in Table 6. Each profile consists of 14 vertical measurement locations, and their elevation from the still water surface is given in Table 7.

Table 6: Profile Particulars of the ADV measurements

prof no	x pos. (m)	y/b	velocity field
1	-4.2	0.25	current only
2	-4.2	0.50	current only
3	-4.2	0.75	current only
4	-4.2	0.75	waves and current
5	-4.2	0.50	waves and current
6	-4.2	0.25	waves and current
7	-2.7	0.25	current only
8	-2.7	0.50	current only
9	-2.7	0.75	current only
10	-2.7	0.75	waves and current
11	-2.7	0.50	waves and current
12	-2.7	0.25	waves and current
13	-1.2	0.28	current only
14	-1.2	0.50	current only
15	-1.2	0.72	current only
16	-1.2	0.72	waves and current
17	-1.2	0.50	waves and current
18	-1.2	0.28	waves and current
19	-0.2	0.34	current only
20	-0.2	0.66	current only
21	-0.2	0.34	waves and current
22	-0.2	0.66	waves and current
23	0.8	0.36	current only
24	0.8	0.64	current only
25	0.8	0.36	waves and current
26	0.8	0.64	waves and current

Table 7: Vertical measurement positions for each velocity profile

pos no.	1	2	3	4	5	6	7
z/h	-0.17	-0.23	-0.29	-0.35	-0.41	-0.47	-0.53
pos no.	8	9	10	11	12	13	14
z/h	-0.59	-0.65	-0.71	-0.77	-0.83	-0.89	-0.95

B Gage positions for the different experiments

Table 8: Gage positions for monochromatic breaking wave tests

gage	1	2	3	4	5	6	7	8	9	10
x pos (m)	-5.2	-4.83	-4.4	-4	-3.61	-3.21	-2.8	-2.4	-2.03	-1.7

gage	11	12	13	14	15	16	17	18	19	20
x pos (m)	-1.4	-1.11	-0.81	-0.5	-0.25	-0.03	0.3	0.6	0.89	1.19

gage	21	22	23	24	25	26	27	28	29
x pos (m)	1.5	1.8	2.17	2.6	3	3.39	3.79	4.3	4.8

Table 9: Gage positions for monochromatic wave reflection tests

gage	1	2	3	4	5	6	7	8	9	10
x pos (m)	-4.6	-1.4	-1.35	-1.3	-1.25	-1.2	-1.15	-1.1	-1.05	-1

gage	11	12	13	14	15	16	17	18	19	20
x pos (m)	-0.95	-0.9	-0.85	-0.8	-0.75	-0.7	-0.65	-0.6	-0.55	-0.5

gage	21	22	23	24	25	26	27	28	29	30
x pos (m)	-0.45	-0.4	-0.35	-0.3	-0.25	-0.2	-0.15	-0.1	-0.05	0

gage	31	32	33	34	35	36	37	38	39	40
x pos (m)	0.05	0.1	0.15	0.2	0.25	0.3	0.35	0.41	0.46	0.51

gage	41	42	43
x pos (m)	0.56	0.61	0.66

Table 10: Gage positions for random wave, wave groups and wave packet tests

gage	1	2	3	4	5	6	7	8	9	10
x pos (m)	-4.6	-2.9	-2.6	-2.3	-2	-1.7	-1.39	-1.09	-0.79	-0.59

gage	11	12	13	14	15	16	17	18	19	20
x pos (m)	-0.39	-0.2	0	0.2	0.4	0.6	0.8	1	1.2	1.4

gage	21	22	23	24	25	26	27	28	29	30
x pos (m)	1.6	1.79	1.99	2.19	2.39	2.59	2.8	3	3.2	3.4

gage	31	32	33	34	35	36
x pos (m)	3.6	3.81	4.01	4.21	4.41	4.61